PRS-UMS-91-004
0 April 1991

Foreign Broadcast Information Service 50 ANNIVERSARY 1941 - 1991

JPRS Report

Science & Technology

USSR: Materials Science

Science & Technology
USSR: Materials Science

JPRS-UMS-91-004 *30 April 1991*

CONTENTS

Nonmetallic Materials

Preparations

Treatments

Welding, Brazing, Soldering

Method for Designing Mirrors for Conversion of a Gaussian Beam

917D0043D Kishinev ELEKTRONNAYA OBRABOTKA MATERIALOV in Russian May-Jun 90 pp 43-45

[Article by V.Ye. Sklyarevich, A.V. Detkov and P.A. Syrovets, Ukrainian SSR Academy of Sciences Electric Arc Welding Institute imeni Ye.O. Paton, Kiev]

UDC 535.312

[Abstract] The equation is obtained for a metal mirror profile which will map a cylindrical Gaussian beam (divergence of about 3|SD) onto a rectangular surface with a uniform intensity distribution. By way of example, a mirror was designed for millimeter-range microwave radiation commonly used in materials heat treating. It converted a 23 mm diameter beam from a source 780 mm from the mirror into a 20 x 200 mm rectangle 250 mm from the mirror, with concentration of 95 percent or more of the incident energy and minimum deviation of six to eight percent. The mirror itself (300 mm along the vertical and 200 mm along the horizontal) was machined on an NC machine tool with a surface finish of less than 0.1 mm from a grid of 200 x 66 points calculated from the given formula. References 4 Russian; figures 2.

Crystallization As the Cause of Microinhomogeneity in Fluorozirconate Glasses

917D0044A Moscow VYSOKOCHISTYYE VESHCHESTVA in Russian Sep-Oct 90 pp 30-49

[Article by M.F. Churbanov and V.S. Shiryayev, USSR Academy of Sciences Chemistry of High Purity Materials Institute, Gorky]

UDC 546:161:54-161.6

[Abstract] In this review, the authors systematize existing data on the kinetics of crystallization on microinclusions and impurities in one class of halide glass, fluorozirconates, which is a primary source of optical losses in optical fibers. Topics include: the resistance of fluorozirconates to crystallization as a function of composition; current experimental methods; crystalline phase content, nucleation rate and rate of linear crystal growth as functions of temperature; and how these kinetic characteristics affect manufacture of optical fibers. It is remarked that the ArF_4 - BaF_2 - LaF_3 - AlF_3 - NaF and ArF_4 - BaF_2 - LaF_3 - AlF_3 - LiF glass systems are most susceptible to crystallization. References 56: 10 Russian, 46 Western; figures 16; tables 7.

The Effect of Impurities on T_c in Y - Ba - Cu - O Ceramics

917D0044B Moscow VYSOKOCHISTYYE VESHCHESTVA in Russian Sep-Oct 90 pp 60-63

[Article by V.M. Azhazha, S.D. Lavrinenko, G.F. Tikhinskiy, and I.N. Tokar, UkSSR Academy of Sciences Physical-TechnicalInstitute, Kharkov]

UDC 538.945

[Abstract] The authors propose that the effect of an impurity in a ceramic on its critical temperature for the superconducting transition in a high temperature superconductor may be represented as $T_c = T^0_c - (dT/dx)c$, where c is the impurity content and dT/dx the change in critical temperature with respect to changes in impurity concentration. The primary impurity elements in commercially-available high purity $Y_1Ba_2Cu_3O_x$ are estimated; these are Na, K, Si, Ca, Al, Ti, Fe, C, N and F. These elements, plus Mg, B, Ge and Zn, were added to solid phase ceramic $Y_1Ba_2Cu_3O_x$ powders to determine their effect on T_c; only carbon and sodium caused modest increase in the superconducting transition temperature. References 10: 4 Russian, 6 Western; figures 2; tables 1.

Magnetic Susceptibility of Thin Coatings Deposited on a Dielectric

917D0044C Moscow VYSOKOCHISTYYE VESHCHESTVA in Russian Sep-Oct 90 pp 72-76

[Article by V.D. Kalugin, V.I. Sheremet, N.S. Opaleva, and S.I. Belyakova (now deceased), Chemistry SRI at Kharkov State University Kharkov, and Metrological SRI imeni D.I. Mendeleyev (A-U) NPO, Leningrad]

UDC 538.214:621.793

[Abstract] The authors measure the specific magnetic susceptibility of thin films of PbS, Cu-Pb and PbS-Pb deposited onto prepared quartz or glass substrates, using a method which finds the para- and diamagnetic properties to within 2 percent. By finding the total magnetic susceptibility of various layer combinations and comparing, the specific susceptibility of the coatings is found, and may be used to monitor the presence of ferromagnetic impurities in the materials for sensitive superconducting magnetic field probes. The susceptibility of the individual components is also tabulated and compared to published values; these vary widely, especially in the case of copper deposited by chemical precipitation onto quartz and glass and containing Ni^{2+} ions, which is lower than published values by 2.5 orders of magnitude. References 10 Russian; tables 2.

Monte Carlo Simulation of an Ar + Kr Free Binary Film

917D0044D Moscow VYSOKOCHISTYYE VESHCHESTVA in Russian Sep-Oct 90 pp 91-94

[Article by Ye.N. Brodskaya and Ye.M. Piotrovskaya, Leningrad State University]

UDC 541.183.2

[Abstract] A liquid Ar + Kr film at 88 K is simulated using Monte Carlo techniques as a large canonical ensemble, with pairwise molecular interactions described by the Leonard-Jones potential. Local density

profiles are calculated and an approximate formula for those profiles obtained. The characteristic minimum thickness of the free binary surface is determined; it increases with increasing Kr content. The components separate at the free surface, with the outer layer in equilibrium with the gaseous medium having higher Ar content. Surface tension is also determined. References 6: 1 Russian, 5 Western; figures 1; tables 1.

Analysis of the Kinetics of Crystals Grown From the Vapor Phase in a Constant Volume System

917D0044E Moscow VYSOKOCHISTYYE VESHCHESTVA in Russian Sep-Oct 90 pp 130-136

[Article by M.P. Belyanskiy, V.I. Dernovskiy, O.I. Tananayeva, and V.P. Zlomanov, Moscow State University imeni M.V. Lomonosov]

UDC 548.522:546.812.24

[Abstract] Mass and linear crystal growth rates as a function of time are analytically derived, based on a diffusion/convection model of mass transfer in the growth of crystals from the vapor phase. These results were verified experimentally by growing PbTe crystals from the vapor phase at pressures ranging from 5590 to 13.3 Pa and photographing the progress of the (100) edge. The experimental results are lower than those predicted, perhaps due to stoichiometric deviations or unaccounted for tellurium in the vapor which increases the total pressure in the system. The theoretical results are in poor agreement with experiment as the argon pressure is lowered to 1.33 Pa. The slopes of the theoretical curves, however, are in good agreement, and are more accurate than other models presented so far. References 6: 5 Russian, 1 Western; figures 3; tables 1.

Flotation-Photometric Determination of the Amount of Silicon in Gallium Without Separating Out the Macrocomponents

917D0044F Moscow VYSOKOCHISTYYE VESHCHESTVA in Russian Sep-Oct 90 pp 223-226

[Article by L.N. Bakina, N.A. Gracheva, Ye.N. Dorokhova, V.I. Lysyakova, V.A. Orlov, and S.V. Sokolov, State Scientific Research and Design Institute of the Rare Earth Metal Industry, Moscow; Moscow State University imeni M.V. Lomonosov; and the Moscow Institute of Steels and Alloys]

UDC 66.046.8:546.681:546.289

[Abstract] The flotation-photometric method was used to determine the amount of silicon impurity in gallium (down to 2×10^{-5} mass percent) from the colored reaction products of reduced molybdenum silicon acid and chromopyrazol II (XII). The compounds, with maximum optical absorption at 590 nm, floated in a toluol-acetone mixture where they were analyzed by a Spekol spectral calorimeter and the concentration deduced from the absorption. The solutions are prepared in a Giredmet autoclave at 250 |SDC which reduced the time needed for sample preparation and the quantity of reagents, and prevented loss of silicon. The dissolving process now takes 2.5 h, measurements 20 to 25 min. References 7 Russian; tables 3.

Determining the Macrocomponents in Silicon and Chromium Films

917D0044G Moscow VYSOKOCHISTYYE VESHCHESTVA in Russian Sep-Oct 90 pp 227-231

[Article by N.M. Shakhverdi, G.A. Miklina, and A.A. Tumanov, Chemistry SRI at Gorky State University imeni N.I. Lobachevskiy]

UDC 543.063:546.2.539.2

[Abstract] A technique is developed for determination of trace amounts of silicon and chromium in chemically-resistant films obtained by evaporation of chromium silicides on polycor substrates. The films are dissolved in a 1:2 solution of dilute Hal and aluminum, or in a 2:1 solution of concentrated sulfuric and phosphoric acids if the films are to be analyzed only in terms of their chromium content. Silicon is determined by the reaction of silicon-molybdenum blue formations using a foreseen solution in isobutanol as a reducer, and chromium is determined by the reaction with diphenylcarbazide. The threshold for silicon detection is 5 micrograms, 1 microgram for chromium, with relative error less than 10 percent at a confidence of 0.95. References 13 Russian; tables 2.

Composites in KamAZ Vehicles

90D0347A Moscow AVOTMOBILNAYA PROMYSHLENNOST in Russian Jun 90 p 9

[Article by R. A. Azamatov, E. S. Sibgatullin, and R. G. Timergaleyev,[1] KamAZ Scientific Technical Center, Polimer Plant, Kiev Construction Engineering Institute, and Kamsk Polytechnic Institute]

UDC 539.3:539.4

[Text] It is said that the most effective way of solving the set of interrelated problems occurring during the design and manufacture of different machines and devices, including motor vehicles, is that of the wide-scale use of new-generation composites.

This principle is undoubtedly true. By using modern mathematical models of the design of both the composites themselves and the products made from them it is truly possible to simultaneously provide the following: high ergonomic, aerodynamic, and other characteristics of the machines; introduction of modern waste-free, ecologically clean technology for manufacturing components and subassemblies; design of an optimal structure possessing good economic, strength, and other indicators; and finally, high competitiveness of products on the foreign and domestic markets.

This is precisely why designers at the KamAZ Production Association, working jointly with scholars from higher educational institutions, scientific research institutes, and specialists from different enterprises, have undertaken extensive work in the area of composites. Specifically, an academic-scientific-production complex has been created at the Kamsk Polytechnic Institute. One of its scientific experimental laboratories is functioning at the plant Polimer. Work is currently underway to design and manufacture from composites such components of KamAZ vehicles as springs, front and rear fenders, fairings, canvas plates, fuel tanks, cardan shafts, etc.

Thus, when creating an improved vehicle drive shaft, a designer is faced with the tasks of minimizing its mass and reducing its susceptibility from atmospheric corrosion and its noise. At the same time, it is naturally necessary to solve the problem of providing the needed shaft strength and rigidity. Ultimately, the search for rational design versions led to integrated use of high-modulus carbon fiber composites and less expensive fiberglass composites, i.e., to hybrid designs.

Let us take a biaxial modification of a drive shaft for a KamAZ vehicle. In the metal version it consists of two parts separated by an intermediate support. The distance between the two end supports equals 3,343.5 mm, the tubes' internal diameter is 94 mm, and their walls are 4 mm thick. In summary, the total mass of the tubes and intermediate support is about 80 kg. One must not remove the intermediate support and replace the two tubes by one; because of vibrations the critical shaft rotation frequency will not be at a high enough level (its rated rotation frequency equals 2,200 min^{-1}).

The picture changes substantially, however, if a switch is made to composite materials. This is especially true since the program system for the computer implemented at the KamAZ makes its possible to optimize the structure of the shaft's composite-fiber system by proceeding from the condition of increasing its critical rotation frequency. (In calculations the shaft's inner diameter, its wall thickness, the distance between supports, the order of arrangement and orientation of the layers of different materials throughout its thickness, and their mechanical properties are taken as the source data).

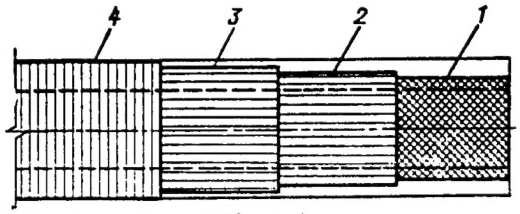

Figure 1.

Figure 1 presents one possible version of organizing the structure of a cardan shaft. There 1 indicates the two inner spiral-crossed layers with an angular orientation of their fibers of +/- 45°, 2 and 3 indicate layers with a lengthwise orientation of the fibers, and 4 indicates a layer having a spiral-annular orientation. The layer labeled 3 is made of high-modulus carbon plastic, whereas the remaining layers are made of fiberglass composite.

3.	1. Характеристика текстурных слоев				2. Характеристика вала				
Номер варианта	4. Номер слоя на рисунке	5. Толщина, мм	6. Модуль упругости, МПа	7. Угол ориентации, град.	8. Внутренний диаметр, мм	9. Толщина стенки, мм	10. Масса, кг	11. Модуль Юнга, ГПа	12. Критическая частота вращения, $мин^{-1}$
1	1	1,2	73	45					
	2	0,4	73	0					
	3	0	377	0	94	4	10,4	51	926
	4	0,4	73	90					
2	1	1,2	73	45					
	2	0,9	73	0					
	3	1,5	377	0	94	4	9,1	165	1778
	4	0,4	73	90					
3	1	1,2	73	45					
	2	0	73	0					
	3	2,4	377	0	94	4	8,3	234	2213
	4	0,4	73	90					
4	1	1,2	73	45					
	2	6,2	73	0					
	3	0	377	0	120	8	27,3	60	1313
	4	0,6	73	90					
5	1	1,2	73	45					
	2	3,6	73	0					
	3	2,6	377	0	120	8	24,2	159	2261
	4	0,6	73	90					
6	1	1,2	73	45					
	2	0	73	0					
	3	6,2	377	0	120	8	20	296	3385
	4	0,6	73	90					

Table 1.

Key: 1. Textured Layes' Characteristics—2. Shaft's Characteristics—3. Version No.—4. Layer No. in Figure 1—5. Thickness, mm—6. Elasticity modulus, MPa—7. Orientation angle, °—8. Inner diameter, mm—9. Wall thickness, mm—10. Mass, kg—11. Young modulus, GPa—12. Critical rotation frequency, min^{-1}

Judging by foreign publications, such shafts, which are intended for lightweight trucks, have manifested good performance qualities. Their structures were therefore selected as data for debugging the programs. Table 1 presents the results of their use.

During the calculations the shaft's length was assumed to equal 3,343.5 mm, and the structure of the composite-fiber system was assumed to equal +/- 45°, 0°, 0°, and 90°. The data presented in Table 1 thus characterize the dependence of a shaft's critical rotation frequency and mass on its inner diameter, wall thickness, and the change in thickness of layers 2 and 3 (i.e., the changes in relative thickness of the carbon plastic layer). Versions 1 through 3 were obtained for the case where the shaft's inner diameter equals 94 mm and the thickness of the bundle of layers equals 4 mm; versions 4 through 6 were obtained for the case where the shaft's inner diameter equals 120 mm and the bundle of layers is 8 mm thick.

As is evident from Table 1, composites make it possible to significantly reduce a shaft's mass and eliminate its intermediate support. In addition, they give a designer the broad capability of optimizing the geometric, physicomechanical, and performance parameters of a shaft in a real design.

Footnote

1. E. A. Gasanov and I. G. Teregulov also participated in this work.

Thermal Expansion of Metals at Low Temperatures

917D0051A Sverdlovsk FIZIKA METALLOV I METALLOVEDENIYE in Russian Jul 90 pp 5-12

[Article by F.I. Dolinin, E.Z. Kuchinskiy, and Ye.A. Pamyatnykh, Urals State University imeni A.M. Gorky]

UDC 536.413

[Abstract] The thermal expansion coefficient of metals at low temperatures is studied using a single-component electron fluid model with random dispersion, and conditions are postulated under which the metal could actually expand as the temperature dropped, as has been observed in heavy fermion compounds and certain ferromagnetic alloys. In particular, the authors look into the effect of the chemical potential and electron interactions on the thermal expansion coefficient when the orbital motions of electrons are quantized in a magnetic field. It is shown that the thermal expansion coefficient may reach anomalously high values at oscillation peaks, depending on whether these oscillations occur over minimum or maximum cross-sections of the Fermi surface. References 24: 12 Russian, 12 Western.

Toward a Microscopic Theory of the Superconductivity of Twinning Planes

917D0051C Sverdlovsk FIZIKA METALLOV I METALLOVEDENIYE in Russian Jul 90 pp 201-203

[Article by S.V. Kuplevakhskiy and I.I. Falko, Kharkov State University imein A.M. Gorkiy, and Kharkov Polytechnic Institute imeni V.I. Lenin]

UDC 537.312.62.001

[Abstract] The authors analyze the microscopic equations to answer objections about the use of a negative sign for a phenomenological parameter γ used in the boundary conditions for an antisymmetric solution to the Ginzburg-Landau equation for the order parameter. A symmetric solution that goes to zero at infinity was found in an earlier theory to explain the intensification of Cooper pairing and hence localized superconductivity at twinning planes. An expression for the critical temperature in terms of the coherence length is found. References 9: 8 Russian, 1 Western.

The Effect of Heat Treating on the Structure and Magnetic Properties of a Rapidly-Solidified Alloy of the Fe-Nd-B System

917D0051D Sverdlovsk FIZIKA METALLOV I METALLOVEDENIYE in Russian Jul 90 pp 53-60

[Article by V.V. Stolyarov, R.Z. Valiyev, A.I. Deryagin, G.F. Korznikova, and Kh.Ya. Mulyukov, USSR Academy of Sciences High- Plasticity Metals Institute]

UDC 669.15.018.58:537.624.8

[Abstract] The effect of temperature and duration of crystallizing annealing on the microstructure, phase content and magnetic properties of rapidly-solidified ribbons of $Fe_{83}Nd_{13}B_4$ alloy is studied. This material is promising as a replacement for cobalt in permanent magnets. the melt was spun onto the chillblock at 20 or 40 m/s, which according to electron microscope data correspond to amorphous/crystalline (magnetically hard) and quasi-amorphous (magnetically soft) states, respectively. A comparative analysis is made of thermal stability and hysteresis properties of the alloys in states with various proportions of amorphous to crystalline phases. Annealing at 600 |SDC for 20 min resulted in complete crystallization with extremely fine-grained structure (50 nm grain size). Increasing this to 750 |SDC for 80 min caused precipitation of excess phases while maintaining the dispersion of the primary $Nd_2Fe_{14}B$ phase and reducing the coercive force. Annealing also sharply increased the hysteresis loop width from 1.5 to 880 kA/m in quasi-amorphous states and from 600 to 1000 kA/m in amorphous/crystalline states, increased the critical temperature by 100 |SDC and lowered the saturation magnetization. References 15: 4 Russian, 11 Western; figures 5; tables 1.

The Effect of Surface Crystallographic Orientation and Thickness on Magnetic Losses and Domain Structure of Fe - 3 Percent Si

917D0051E Sverdlovsk FIZIKA METALLOV I METALLOVEDENIYE in Russian Jul 90 pp 67-76

[Article by V.F. Tiunov, Urals Branch of the USSR Academy of Sciences Metals Physics Institute]

UDC 538.221:669.14.018.583

[Abstract] The authors study the effect of equilibrium domain structure and its dynamic behavior upon refinement of Fe - 3 percent Si single crystals with various surface crystallographic orientations. These characteristics are used for analysis of eddy-current losses as a function of sheet thickness for magnetic field strengths from 0.5 to 1.9 T. It is shown that the domain width decreases in [001](011) single crystals upon reversal of magnetization, while on the other hand it increases in where the magnetization is misaligned with respect to the surface by 1°. The process of remagnetization in sheets 0.14 mm and greater in thickness was accompanied by noticeable breakdown of domain structure, intensifying with increasing magnetic field strengths. This behavior was not apparent for thicknesses less than 0.07 mm. It is argued that the eddy-current losses in thin single crystal sheets are governed only by the domain width and nonuniformity in the rates of grain boundary displacements. References 15: 7 Russian, 8 Western; figures 5; tables 1.

Crystallization in Amorphous FeCoBSi Alloys

907D0187A Moscow IZVESTIYA VYSSHIKH UCHEBNYKH ZAVEDENIY: CHERNAYA METALLURGIYA in Russian Vol 19 No 6, Jun 90 pp 106-107

[Article by B. V. Zhalnin and R. I. Malinina, Moscow Institute of Steels, Alloys]

UDC 539.213

[Abstract] A study was made of the crystallization of amorphous $(FeCo)_{80}(BSi)_{20}$ alloys with a change in the ratio of transition elements with $c_{Co}/c_{Fe} = 0.1 - 0.35$. The crystallization temperature and Curie point were determined by thermomagnetic analysis with differential recording of continuous heating at 20 K/min in a magnetic field of 32 kA/m. Quantitative phase analysis was performed. Crystallization was found to be accompanied by diffusion redistribution of silicon among the phases formed. The type of boride formed depends significantly on the magnetic state of the amorphous matrix before crystallization. Figure 1.

Cast Composite Tools

907D0187B Moscow IZVESTIYA VYSSHIKH UCHEBNYKH ZAVEDENIY: CHERNAYA METALLURGIYA in Russian Vol 19 No 6, Jun 90 p 109

[Article by A. A. Baranov, A. G. Lyubchenko, and V. V. Pashinskiy, Donetsk Polytechnical Institute]

UDC 669.018.25

[Abstract] The quality of a blank used for the manufacture of tools can be improved by three-dimensional reinforcement by means of carbon steel inserts. The inserts act as coolers, helping to decrease the grain size of the primary cast structure. The problem of producing defect-free castings with strong bonds was solved by varying the reinforcement factor, the ratio of the volume of the inserts to their surface area, and the temperature conditions of casting the steel. An experimental batch of tools was produced from cast composite blanks consisting of R0M5ST high-speed steel reinforced with 6 - 6.5 mm-diameter bars of low- and medium-carbon steels. The reinforcement representing seven to eight percent of the blanks. Studies of the microstructure of specimens showed that the reinforcement had a favorable influence on reducing carbide heterogeneity, with the matrix containing martensite, carbides and two to five percent residual austenite. The hardness of the tools after final processing was HRC 63 - 64. Figure 1.

Influence of Stochastic Nature of Steel Production on Technical-Economic Characteristics of Steelmaking

907D0187C Moscow IZVESTIYA VYSSHIKH UCHEBNYKH ZAVEDENIY: CHERNAYA METALLURGIYA in Russian Vol 19 No 6, Jun 90 pp 109-110

[Article by Yu. N. Bulanov and V. Ya. Medikov, Siberian Metallurgical Institute]

UDC 669.013.5

[Abstract] Only 18.4 percent of steel is produced by continuous casting, and its usage factor is not over 70 percent. The authors have attempted to study the relationship and mutual influence of certain factors on the operation of a steelmaking shop using continuous casting and the formation of its primary technical and economic characteristics. A diagram is presented illustrating the influence of such factors as melt mass, length and tapping temperature and chemical composition on the economic characteristics of a shop. The results indicate that maximizing the mean number of melts in a series does not always increase the effectiveness of operation of the system. The criterion of effectiveness must be not simply the number of melts achieved, but rather the economic characteristics such as specific adjusted cost. The results of this study can be used to develop plan of measures to improve the utilization of equipment in steelmaking shops. Figure 1, reference 1.

Chrome-Reduction Method of Making Corrosion-Resistant Steel in a Converter

907D0186A Moscow STAL in Russian No 6, Jun 90 pp 18-21

[Article by M. V. Kolesnikov, G. S. Kolganov, P. I. Yugov, and A. B. Khmelevskoy, Central Scientific Research Institute of Ferrous Metallurgy, "Tulachermet" Scientific-Production Association]

UDC 669.14.018.8:669.184

[Abstract] A technology has been developed for production of corrosion-resistant steel in a converter with combined blowing of the bath, including plasma heating and roasting of unconditioned chrome ore and lyme in the converter; pouring of a carbon charge preliminarily melted in the same converter onto the roasted ore and lyme; oxidation-reduction refining of the charge in order to produce a gas-slag-metal emulsion and remove phosphorous in the gas phase; blowing of a high-temperature gas mixture for further reduction of the chrome and manganese; tapping and pouring of the steel. The distinguishing feature of this technology is the smooth transition from oxidation to reduction stages in refining, eliminating sharp changes in temperature during the course of the melt, increasing the life of the lining, decreasing chrome loss and allowing the use of the advantages of the single-slag converter process. A series

of experimental melts were produced by this process in the converter and by a duplex process involving a converter and electric furnace. The use of the high temperature gas mixtures intensifies the oxidation-reduction refining and yields a steel with low content of impurities. The process can be introduced without great capital expense and can be performed in existing converter shops after some reconstruction.

Decarburization in Vacuum-Oxygen Refining of Corrosion-Resistant Steel

907D0186B Moscow STAL in Russian No 6, Jun 90 pp 21-22

[Article by N. S. Grigoryev, Ye. A. Nechayev, G. S. Kozlov, V. P. Liventsev, and V. G. Perfilyev, Cherepovets Metallurgical Combine, Cherepovets Affiliate, Vologodskiy Polytechnical Institute]

UDC 699.014.4:65.011.56

[Abstract] The authors organizations have developed and introduced to production a system for monitoring the oxidation level of waste gases using a standard measurement cell. The gas is collected from a vacuum line. It is found that the time when the oxygen is blown through the metal is important to reduce chrome loss. Monitoring of the oxygen content of the waste gases can be used to determine the correct moment to start and stop the oxygen blow. Figures 2.

Increasing Effectiveness of Nickel Utilization in Making of Corrosion-Resistant Steel

907D0186C Moscow STAL in Russian No 6, Jun 90 pp 25-27

[Article by V. M. Shifrin, A. D. Pereverzev, K. P. Verbitskiy, A. F. Startsev, and V. N. Turovskiy Dnepropetrovsk Metallurgical Institute, "Dnepropetstal" Plant]

UDC 669.187.25

[Abstract] A study of 63 melts used in manufacturing chrome-nickel corrosion-resistant steel in basic arc furnaces by remelting of scrap with blowing of oxygen has shown that most of the nickel is lost during the period of melting and oxygen blowing. This is due to the evaporation of nickel in the arc zone as the furnace operates at high power, which is typical of the melting period. Thermodynamic calculation of the processes of oxidation of carbon and chromium in the melt show that increasing the nickel content in the metal improves the conditions for selective oxidation of carbon. A technology has been suggested for making corrosion-resistant steel involving removal of almost all metallic nickel from the scrap charge, with its addition to the liquid metal upon completion of the oxygen blow. Two series of experimental melts were conducted to test this suggestion. The use of metallic nickel as a cooling and alloying additive reduced its losses in the melting processes by 0.3 percent, increased furnace lining life, improved the quality of the metal and somewhat stabilized titanium loss. Conditions have thus been created for further improvement in the process. Figures 3, references 5: Russian.

Increasing Utilization of Chromium in Melting Corrosion-Resistant Steel Using Copper-Aluminum Anodic Precipitates

907D0186D Moscow STAL in Russian No 6, Jun 90 pp 27-29

[Article by M. I. Gasik, A. Z. Shevtsov, V. A. Shevchenko, Ye. O. Ostreyko, and I. A. Semenov, Dnepropetrovsk Metallurgical Institute, "Dnepropetstal" Plant]

UDC 669.187.25

[Abstract] A study is made of the problem of increasing the degree of extraction of chromium from the post-blow slag by utilization of a complex aluminum-containing alloy deoxidizer in the system Al-Me, the density of which is greater than that of the slag but less than that of the liquid steel. The metal component can be copper, the density of which is three times greater than that of the slag and 1.3 times greater than that of the liquid steel. The relative contact surface of the lumps of solid copper-aluminum alloy with the deoxidized slag was used to determine the effectiveness of utilization of the deoxidizer. It is found that the use of wastes from electrolytic refining of aluminum, an anodic copper-aluminum alloy precipitate, can increase the degree of utilization of chromium and aluminum in the production of corrosion-resistant steel, partially reducing the consumption of cathodic copper. Figures 2, references 6: 5 Russian, 1 Western.

Industrial Testing of New Technology for Producing VSt3sp Steel With Superior Cold and Corrosion Resistance

907D0185A Moscow STAL in Russian No 5, May 90 pp 74-77

[Article by A. Yu. Shulte, L. F. Kosoy, D. A. Litvinenko, V. P. Kharchevnikov, V. A. Sakhno, and O. V. Nosochenko, Physical-Mechanical Institute Scientific, Technical Complex, Ukrainian Academy of Sciences; Central Scientific Research Institute of Ferrous Metallurgy, "Azovstal" Metallurgical Combine]

UDC 621.746.58

[Abstract] The new steel was made in a 350 ton converter, poured by the continuous method and rolled into a sheet on a 3600 mill. Desulfuration was performed in three stages: by blowing a jet of compressed air containing granulated magnesium through the saturated cast iron, as the steel was tapped from the converter by processing in the ladle with liquid synthetic slag and subsequent blowing of silicocalcium powder in a jet of argon. This last operation also modified the metal with calcium, yielding a final sulfur content of not over 0.006 percent, calcium content 0.003 - 0.007 percent. Metallographic analysis was performed according to the state standards. The new steel, called VSt3sp, thanks to the desulfuration, modification and optimal heat treatment, has superior impact toughness and cold resistance. It is

also superior in corrosion-mechanical strength. It has been used to replace traditional low-alloy structural steels. Figures 2, references 4: 3 Russian, 1 Western.

Defects in High-Speed Steels Made of Melted Powders

907D0185B Moscow STAL in Russian No 5, May 90 pp 93-95

[Article by G. I. Parabina and L. N. Marchenko, Ukrainian Scientific Research Institute of Special Steels]

UDC 621.762.4

[Abstract] A study is made of defects related to the quality of the initial powder used in the manufacture of high-speed steels. The appearances described of powder with high oxygen content, nonmetallic inclusions such as bits of furnace slag and liner, foreign powder particles and structural banding. The effects of these defects on the quality of the high-speed steel produced are described. Figures 4, references 10: 8 Russian, 2 Western.

Influence of Defects and Impurities in Diamonds on Their Stability in Gas Oxidizing Media

907D0190A Kiev SVERKHTVERDYYE MATERIALY in Russian No 3, May-Jun 90 pp 5-10

[Article by I. I. Kulakova and A. P. Rudenko, Moscow State University]

UDC 549.211+542.943

[Abstract] A study was made to determine the significance of certain individual peculiarities of diamonds in their behavior in oxidizing media. The influence of other properties was either considered or leveled to the greatest possible extent. Oxidation resistance of crystals of natural diamond with various concentrations of impurity centers and synthetic diamond crystals differing in their content of paramagnetic nitrogen and ferromagnetic inclusions, chemical nature of other impurities and inclusions was studied. Studies were performed under isothermal conditions at atmospheric pressure, 973 - 1323K. The influence of impurity nitrogen centers on the resistance of diamonds to the effects of oxidizers was studied using natural diamond crystals of both pure and mixed types, as determined by IR absorption spectra. It is found that the influence of defects and impurities on the resistance of diamond to oxidation cannot be uniform and depends both on their nature and on the properties of the diamond crystals and the reaction medium. Figures 2, references 8: Russian.

Force in Diamond Grinding of Tools Ceramics

907D0190B Kiev SVERKHTVERDYYE MATERIALY in Russian No 3, May-Jun 90 pp 48-51

[Article by V. I. Lavrinenko, V. V. Shklyarenko, and A. A. Sytnik, Institute of Superhard Materials, Ukrainian Academy of Sciences; Svetlovsk Hard Alloy, Refractory Metal Combine]

UDC 621.923:666.3:621.922

[Abstract] A study is made of the influence of processing modes and type of ceramic processed on the cutting force arising in diamond grinding of tool ceramics. In addition to the components of the cutting force, their resultant, abrasive cutting factor and specific work of grinding were determined. In later experiments different types of ceramics and other materials for comparison were also tested in the same manner. It was found that as the longitudinal and transverse feed rates increased, the cutting forces increased, while the specific work decreased. The abrasive cutting factor decreased for oxide-carbide ceramic and increased for oxide ceramic. As the speed of the disk increased, the specific cutting work increased, while the force decreased. Tool materials can be divided into groups depending on specific work and abrasive cutting factor, which depend on the nature of the material. Figures 2, reference 1: Russian.

Diamond Grinding of Plasma Ceramic Coating

907D0190C Kiev SVERKHTVERDYYE MATERIALY in Russian No 3, May-Jun 90 pp 57-61

[Article by A. M. Plipenko, Cherkassk Affiliate, Kiev Polytechnical Institute]

UDC 621.923.02:621.921.34:666.233

[Abstract] A coating of Al_2O_3 plus 13 percent TiO_2 was atomized onto specimens in a 28 V arc at 600 A, plasma temperature 7000 K, plasma jet speed 730 m/s. The geometric characteristics of the surface layer of the plasma ceramic coatings were determined after diamond disk polishing. The surface parameters were virtually the same after polishing with a diamond disk and belt. Tool type must therefore be selected on the basis of economic considerations. Optimal longitudinal grinding modes were defined: rough grinding—part speed 35 m/min, disk speed 28 m/s, feed rate 0.6 m/min, transverse feed 0.03 mm/pass; finish grinding—part rotation speed 45 m/min, disk speed and longitudinal feed same, transverse feed 0.01 mm/pass. The introduction of diamond grinding of plasma ceramic coatings on various parts has yielded a savings of 200,000 rubles per year at two plants alone. Figures 4, references 5: 4 Russian, 1 Western.

The Effect of Method Used for Manufacturing Zirconium Dioxide Ceramics on Mechanical Strength

917D0041A Moscow OGNEUPORY in Russian Sep 90 pp 8-12

[Article by Ye.I. Akselrod, R.Ye. Volfson, N.M. Chudnova, V.N. Pavlik, I.F. Usatikov, Ye.B. Loyenko, Ukr-NIIO [Refractories SRI (Ukraine)]; and S.G. Titov and V.Ye. Chernov, VNIImetmash [Metallurgical Machine Building SRPDI (A-U)]]

UDC 666.762.52.017:620.174

[Abstract] This article presents the results of bending strength tests of zirconium dioxide ceramics depending on the type of additives used to stabilize the ZrO_2 (including Y_2O_3 and MgO), the stabilization method, and the method used to form and fire the samples. The following manufacturing methods were tried: dry-press molding, hydrostatic molding, hot molding, isostatic hot molding, and slip casting. Three- point bending strength tests were conducted by a method developed at Ukr-NIIO, and its setup is described. The Weibull modulus and temperature dependence of ultimate bending strength were also determined. It is remarked that the strongest samples are those obtained by hot isostatic molding at 1400 - 1500°C of grade TsI-6 powder made by coprecipitation from an aqueous solution of zirconium and yttrium salts. Mechanical treating of the surface increases the strength by 20 percent and nearly

doubles the Weibull modulus; firing at 1200 °C is also considered optimal. References 5: 3 Russian, 2 Western; figures 2; tables 4.

Structural Ceramic Materials Based on Reactivity-Constrained Silicon Nitride

917D0041B Moscow OGNEUPORY in Russian Sep 90 pp 13-18

[Article by V.V. Vikulin and I.N. Kurskaya, Tekhnologiya ONPO]

UDC 666.762.93

[Abstract] Ceramics based on reactivity-constrained silicon nitride (RCSN) can maintain their structural strength at temperatures up to 1400°C in air, have low coefficient of thermal expansion, can withstand abrupt thermal cycling loads, and are relatively easy to manufacture in terms of raw materials supply and ecological impact. RCSN is formed by nitriding finely-dispersed silicon powder with nitrogen gas at 1400 - 1500°C. A matrix regression model is used to determine optimum conditions for manufacturing ceramics from RCSN; long-term strength of the oxidation-resistant RCSN-based material OTM - 904 is tested and the results tabulated. The effect of boron doping of the silicon powder, thermal conductivity as a function of temperature, and other important physical and chemical properties are discussed. References 8: 6 Russian, 2 Western; figures 4; tables 2.

Ceramics Made From Alumiomagnesial Spinel Obtained From a Solar Heated Melt

917D0041C Moscow OGNEUPORY in Russian Sep 90 pp 19-21

[Article by G.T. Adylov, B.Ye. Bibersheyn, G.V. Voronov, and E.M. Urazayeva, Fizika-Solntse NPO Physical-Technical Institute]

UDC 666.762.36.046.4

[Abstract] This article studies the result of synthesis of $MgO.nAl_2O_3$ in a solar furnace. The characteristics of the sintering of the ceramic from melted spinel grains depending on the grain content and activating sintering of additives are also examined. The results indicate that samples with stoichiometric spinel content sintered better than those with excess aluminum oxide. Use of activating sintering additives reduced the open porosity of the spinel samples from 15 to 0.15-1.5 percent. References 4 Russian; figures 1; tables 3.

The Effect of Technological Factors on the Manufacture of Ingots With Mullite or Mullite-Corundum Composition

917D0041D Moscow OGNEUPORY in Russian Sep 90 pp 21-28

[Article by V.A. Ustichenko, N.V. Pitak, and V.S. Shapovalov, Refractory SRI (Ukraine)]

UDC 666.762.14.046.4

[Abstract] A mullite melt in an arc furnace contains a mixture of SiO_2 and Al_2O_3 in contact with solid carbon. It was found that synthesis of mullite differing very little in content from the initial mixture may be obtained in an OKB - 514 arc furnace at 194 V/1800 A, although this setting is very sensitive; increasing the voltage leads to significant changes in composition due to reduction of part of the SiO_2 and a resulting mullite-corundum content. Most of the SiO_2 during melting is lost in the initial phase. For an alumina:silica ratio of less than 3.5, crystallization of mullite had a very directional character, going from the chilled surface toward the center of the ingot. Zonal structure is seen at alumina:silica ratios between 3.5 and 4.5, and above this there is a fine-grained structure made up of prismatic and isometric corundum and mullite. References 13: 10 Russian, 3 Western; figures 14; tables 4.

The Formation of Nonplastic Corundum

917D0041E Moscow OGNEUPORY in Russian Sep 90 pp 30-33

[Article by I.A. Dmitriyev, M.I. Podkovyrkin, L.G. Beloborodova, T.M. Kleshcheva, and Ye.S. Gorskaya, Urals Polytechnic Institute]

UDC 666.762.11.032.656

[Abstract] The mechanism of plasticization in nonplastic compounds is studied. The authors examined the effect of a variety of complex plasticizing agents (dextrin, methylcellulose, synthetic rubber) on the formation of a high-silica compound. The behavior of the components of these plasticizing agents during heat treating is investigated. It is shown possible to make items from nonplastics by extrusion using complex binders. References 6 Russian; figures 2; tables 1.

Blue Light Systems in Diamond

907D0189A Kiev SVERKHTVERDYYE MATERIALY in Russian No 2, Mar-Apr 90 pp 3-8

[Article by Ye. V. Sobolev and O. P. Yuyeva, Institute of Inorganic Chemistry, Siberian Affiliate, USSR Academy of Sciences]

UDC 549.211:535.37

[Abstract] A number of systems have been classified in blue-light diamonds by studying several thousand specimens from various sources. The relaxation characteristics and temperature variation of intensity have been determined, oscillating structure studied and comparisons conducted with IR and UV absorption, EPR, thermally stimulated luminescence, X-ray and cathode luminescence studies. Ten systems in all are found in natural diamond crystals. The electron transitions responsible for blue light involve trivalent substituted diamond atoms with unshared two s-electron pairs and carbon radicals as centers. Both point centers and other nitrogen-vacancy complexes take part in formation of blue light, as well as nitrogen segregations and dislocations, forming unstructured bands. Large centers as sets of identical fragments characteristically show floating of levels into a zone, which explains the appearance of loops and the unstructured nature of the bands, as well as the changes in spectral composition of the light with various excitation methods. Figures 4, references 16: 13 Russian, 3 Western.

Impurity Absorption Spectra and Conductivity Activation Energy of Synthetic p-Type Diamonds

907D0189B Kiev SVERKHTVERDYYE MATERIALY in Russian No 2, Mar-Apr 90 pp 8-13

[Article by V. A. Davydov, M. I. Yeremets, O. G. Revin, and V. V. Struzhkin, Institute of High-Pressure Physics, USSR Academy of Sciences]

UDC 631.315.592

[Abstract] A study is made of the results of investigation of impurity absorption spectra and activation energy of impurity conductivity in synthetic diamonds. The p-type diamonds contained boron from 10^{16} to 10^{20} cm^{-3}. Analysis of the spectra considering the lattice absorption of diamond is used to determine an additional peak in the impurity absorption system at 0.291 eV, related to the absorption spectrum of an acceptor center. Comparative analysis of impurity systems of diamond and germanium is used to identify the activation energies of impurity conductivity in the diamond. Figures 3, references 16: 6 Russian, 10 Western.

Structure and Wear Resistance of Silicon Carbide-Aluminum Nitride System Ceramics

907D0189C Kiev SVERKHTVERDYYE MATERIALY in Russian No 2, Mar-Apr 90 pp 28-31

[Article by V. A. Melnikova and V. K. Kazakov, Institute of Material Science Problems, Ukrainian Academy of Sciences; Institute of Superhard Materials, Ukrainian Academy of Sciences]

UDC 621.921:620.187

[Abstract] A study is presented of the influence of microstructure and mechanical properties of materials in the system SiC - AlN on their friction parameters. Specimens produced by hot pressing at 1800°C from technical aluminum nitride and silicon carbide powder with particle size not over 3 μm. The study of hot pressed two-phase SiC - AlN composites establishes the relationship between structure, mechanical and friction properties. The wear mechanism is found to be primarily related to crack formation in the surface layer. The quantity of substance lost to friction is determined in the final analysis by the hardness and toughness of fracture. By varying the composition of two-phase composites it becomes possible to change their dispersion, defect content and other microstructural parameters over wide limits, achieving good strength properties and maximum wear resistance. Figures 3, references 5: 4 Russian, 1 Western.

Formation of Composite Coatings Containing Microscopic Diamond Powder

907D0189D Kiev SVERKHTVERDYYE MATERIALY in Russian No 2, Mar-Apr 90 pp 46-50

[Article by T. M. Duda, A. A. Elbert, Ye. L. Prudnikov, and L. A. Leneva, Institute of Superhard Materials, Ukrainian Academy of Sciences]

UDC 621.921.021:666.233

[Abstract] A study is presented of the specifics of formation of composite electrochemical and chemical coatings of electrolyte suspensions containing microscopic diamond powder with a change in various process parameters. The formation of electrochemical coatings based on nickel and a cobalt-nickel alloy and chemical coatings based on a nickel-phosphorous was studied upon precipitation with microscopic diamond powder, grain size 3/2 to 14/10. The experiments were used to determine the influence on composition of the coating produced of the current density, diamond particle concentration in the suspension, their granularity, the matrix material and the coprecipitation time. The total quantity of electricity expended in the production of the electrochemical coatings was recorded. It is determined that in order to increase the quantity of diamond grains in the coatings it is necessary to select the current density and dispersed phase concentration in the electrolyte as functions of powder grain size. The optimal content of particles of large dimensions occurs at higher current density and dispersed phase concentration than is required for smaller particles. The capacity of the matrix for inclusion of diamond powder decreases in the sequence Ni - P, Ni - Co, Ni. Precipitation of matrix metal onto the surface of conducting inclusions in the diamond powders changes the physical properties of the grains and significantly influences the kinetics of formation of electrochemical coatings. Figures 4, references 6: Russian.

Third Seminar 'Electron Paramagnetic Resonance and Optical Spectroscopy of Defects and Impurities in Diamond'

907D0189E Kiev SVERKHTVERDYYE MATERIALY in Russian No 2, Mar-Apr 90 pp 65-67

[Article by L. A. Shulman and V. G. Malogolovets]

[Abstract] An inter-industry scientific seminar dedicated to the study of defects and impurities in diamonds by electron paramagnetic resonance and optical spectroscopy was held 18-20 October 1989 in Aleksandrovo (RSFSR, Vladimir Oblast). Subjects discussed included the state of impurity hydrogen in the diamond lattice; modification of the defect and impurity structure of diamond and cubic boron nitride upon ion implantation over a broad energy range; EPR studies of paramagnetic centers in ion-implanted diamond layers; electrically active impurity centers and structural defects in ion-implanted diamond; studies of diamond films grown on tungsten substrates; luminescence of natural diamonds upon laser excitation; heat and pressure treatment of diamonds; the effect of impurity centers and defects on the abrasive strength of diamonds; synthetic diamonds produced by recrystallization and containing large spherical cavities; microwave photoconductivity of natural diamonds; distribution of capture centers in synthetic diamond; heat conductivity of diamonds; X-ray topographic studies of diamonds; and the influence of dislocations on the optical absorption spectra of natural diamonds. The next seminar is planned for 1991.

Graphite Content's Influence on Tribotechnical Characteristics of Copper- Coppered-Graphite Powder Systems

917D0014A Minsk IZVESTIYA AKADEMII NAUK BELORUSSKOY SSR: SERIYA FIZIKO-TEKHNICHESKIKH NAUK in Russian No 2, 1990 (manuscript received 16 Oct 89) pp 34-36

[Article by V. A. Kovtun, V. G. Savkin, L. A. Anistratenko, and V. B. Shuvalov, Institute of Mechanics of Metal-Containing Polymer Systems, Belorussian SSR Academy of Sciences]

UDC 621.891:620.22

[Text] Metal-and-graphite composites have the property of a self-lubrication character and are finding ever greater application in assemblies operating under dry friction, in various gaseous media and under the influence of temperature fields. These materials are also being used in motor commutator brush units and electric transport current collection units.

The graphite content is usually not greater than 2 to 5 percent by weight in known metal-and-graphite composite antifriction materials, in association with the necessity of preserving their strength characteristics and reducing the amount of wear.[1] However, this quantity of dry lubricant is insufficient for guaranteeing the normal operation of rubbing assemblies, in particular, for guaranteeing a low and constant coefficient of friction.

In the opinion of a number of researchers,[2,3] in order to improve the operating characteristics of metal-and-graphite composites the metal in them must form a continuous matrix, and the graphite must be in the form of isolated inclusions. The use in the above-cited composites of pre-metal-coated graphite particles assists in producing such a structure.

This applies first of all to copper - coppered-graphite powder composites, which are now attracting the attention of a circle of researchers. This interest is due to the fact that these materials have higher than usual tribotechnical and operating characteristics because of the additional number of metallic contacts between the particles of the copper of the matrix and the copper shells of the coated graphite.[4,5] However, the operating properties of copper-and-graphite materials as a function of the graphite content have been studied insufficiently.[6] A tribological assessment of the service characteristics of these materials is quite timely.

In this paper a study is made of the graphite content's influence on the tribotechnical characteristics of thin-film coatings of copper - coppered-graphite powder system materials.

The coatings were produced by the method of the electric-contact baking of a powder material onto a metallic substrate, during which mechanical pressure is applied to the composite at the same time and electrical current is passed through.[7] The constituent components of the coatings were GOST [All-Union State Standard] 4960-75 type PMS-1 copper powder and type GMP graphite granules chemically coppered with a particle dimension range of 100 to 200 μm. The 3 - to - 7 - μm - thick copper film on the graphite particles had a dendritic structure. The powder systems were prepared by mechanical mixing of the components.

GOST 1173 - 77 type DPRNM - 0.2 x 15 NDM - 3 copper ribbon was used as the metallic substrate, and the coatings were applied on a unit made to order on the basis of a resistance welder. The use of a feeder in the production process made it possible to control precisely the coating's thickness and assured the uninterrupted application of the disperse composite to the metallic ribbon. The coating of the specimens tested was 90 to 100 μm thick.

The specimens were tested for eight hours on the SMT-1 machine under sliding friction according to a shaft - partial-bushing scheme under a load of 200 kPa and a speed of 1 m/s. Type 45 steel having a hardness of HRC 44 and surface roughness of R_a = 0.63 μm acted as the mating surface's material. Each tribotechnical characteristic value represents the average of three measurements.

The relationship between the coating specimens' coefficient of friction and wear rate and the graphite content is shown in Figure 1.

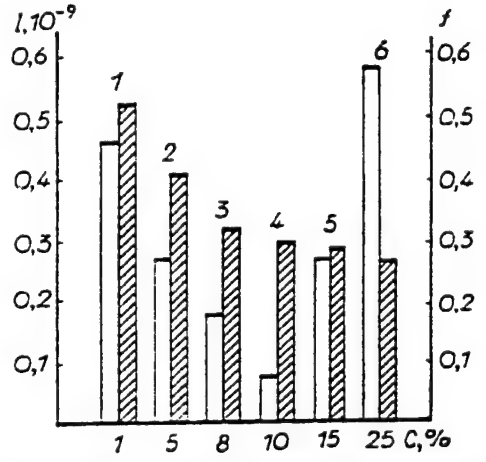

Figure 1. Relationship Between Coating Specimens' Coefficient of Friction, f, (Hatched) and Wear Rate, I, and Graphite Content

It was established that the coatings' coefficient of friction decreases monotonically as the graphite content increases from 1 to 25 percent by weight. At the same time, the wear rate's dependence on the graphite content has an extremum character. Coatings having a graphite content on the order of 10 percent by weight have the minimum wear rate, and a growth is observed in the wear rate as the graphite content increases further. In a coating having a graphite content of 15 percent by weight

(specimen No. 5) the wear rate reaches the level of a coating containing only 5 percent by weight of graphite (specimen No. 2). However, while the difference between the coefficients of friction of specimens Nos. 6 and 4 is only 5 to 10 percent, their wear rates differ by a factor of eight (Figure 1).

Studies of the wear products of the materials on a scanning electron microscope showed that copper particles affixed to the graphite particles formed in the friction process are distinctly visible on the surfaces of these graphite particles. As the graphite content increases, the quantity of copper on the surface of the wear particles gradually increases and reaches its maximum value with a graphite content of 10 percent by weight in the coating material (Figure 2a). A reduction in the quantity of affixed copper particles is observed on the surface of wear particles of coppered graphite formed during friction for a coating having a high graphite content (Figure 2b).

Caption: Figure 2. Photographs of Surface of Graphite Particles Formed in Process of Wear of Coatings With Graphite Content of 10 (a) and 25 (b) Percent by Weight, 3000X [Figure not reproduced]

In analyzing the results presented, it can be noted that a high coefficient of friction (as much as 0.5) and intense wear of the material are observed during frictional interaction with a graphite content in the system of less than 5 percent by weight, because the added graphite is insufficient for the formation of a fit film of lubricant on the rubbing surface, and the material's significant heterogeneity contributes to redistribution of the load on various elements of the system and to the easy separation (breaking off) of graphite particles from the metallic matrix.

Favorable conditions for lubrication of the rubbing working surfaces are created (a coefficient of friction on the order of 0.2) with a high graphite content (greater than 10 percent by weight). However, the strength of the bond of the coppered particles of graphite in the metallic matrix is reduced at the same time because of the presence of a large amount of direct contact of filler particles with one another and the disruption of the matrix material's continuity because of this.

Thus, the studies conducted demonstrated that for copper - coppered-graphite sintered powder systems there is an optimum ratio of components (approximately 10 percent by weight of graphite in the case examined) that guarantees a sufficiently low coefficient of friction and minimum wear rate, and this ratio is due to the competing influence of the processes of improvement of the lubrication of the working surfaces and the change in the strength of the bond of the graphite particles in the metallic matrix.

Bibliography

1. Fedorchenko, I. M. and Pugina, L. I., "Kompozitsionnyye spechennyye antifriktsionnyye materialy" [Sintered Composite Antifriction Materials], Kiev, 1980.

2. Balshin, M. Yu., "Poroshkovoye metallovedeniye" [Powder Metallurgy], Moscow, 1948.

3. Dzhons, V. D., "Osnovy poroshkovoy metallurgii, svoystva i primeneniye poroshkovykh materialov" [Powder Metallurgy Basics, Properties and Application of Powder Materials], Moscow, 1965.

4. Yas, D. S., Pavlenko, V. I., and Podmokov, V. B., POROSHKOVAYA METALLURGIYA, No 1, 1976, pp 31-34.

5. Kuzmina, I. V., Belyayeva, G. I., Pastukhov, V. P., and Frishberg, I. V., POROSHKOVAYA METALLURGIYA, No 7, 1985, pp 96-100.

6. Nichiporenko, O. S., Braterskaya, G. N., Medvedovskiy, A. G., et al., POROSHKOVAYA METALLURGIYA, No 2, 1986, pp 63-68.

7. Dorozhkin, N. N., Abramovich, T. M., and Yaroshevich, V. K., "Impulsnyye metody naneseniya poroshkovykh pokrytiy" [Impulse Methods of Applying Powder Coatings], Minsk, 1985.

Development of Powder Composites for Glass-Molding Tools

917D0014B Minsk IZVESTIYA AKADEMII NAUK BELORUSSKOY SSR: SERIYA FIZIKO-TEKHNICHESKIKH NAUK in Russian No 2, 1990 (manuscript received 9 Aug 89) pp 37-40

[Article by I. I. Krasnyakov, L. N. Dyachkova, M. M. Dechko, and Ye. V. Zvonarev, Belorussian Republic Powder Metallurgy Scientific Production Corporation]

UDC 621.762

[Text] Glass-molding tools work under complex conditions, such as treatment by thermal cycles, interaction with a glass melt containing abrasive particles, and impact loads. That is why the material of glass molds must possess a combination of satisfactory mechanical, thermophysical and process (processability) properties. In addition, the material's coefficient of thermal expansion must be close to that of the cast iron presently used for making glass molds. It has a number of shortcomings, in particular, higher than usual porosity in castings as their dimensions increase, the occurrence of growth concluding in an irreversible change in the volume of cast iron parts under conditions of higher temperatures than usual, a sharp drop in strength and ductility properties when being used at temperatures of 450 to 500°C, higher embrittlement than usual, and the short life of the molds.

A study was made of the feasibility of replacing cast iron glass-molding tools with powder-composite for the purpose of improving the reliability and performance of glass-making equipment.

Table 1. Experimental Design Matrix and Properties of Materials

No	Composition	Relative Density, θ, %	Sintering Temperature, °C	Hardness, HB	σ_B*, MPa	σ_i*, MPa	a_n*, J/m^2	Wear, L, mm: P = 5 kg*, τ = 10 min	Wear, L, mm: P = 10 kg*, τ = 5 min	CTE: 400 °C	CTE: 600 °C	CTE: 800 °C
1	ZhGr1, 5Kh6G1, 5N4MD7	50	1200	107	350	400	145	2.5	4.3	19.4	20.6	21.7
2	ZhGr1, 5Kh6N4D2	65	1200	170	353	515	143	2.05	4.1	19.6	20.5	20.7
3	ZhGr0, 5Kh6MD7	85	1200	380	575	1012	37	2.8	3.85	13.8	14.8	12.5
4	ZhGr0, 5Kh6G1, 5D2	75	1200	283	384	943	37	5.7	4.0	13.8	15.6	14.0
5	ZhGr1, 5Kh6MD7	75	1150	185	340	441	87	3.0	3.15	18.1	18.7	18.1
6	ZhGr1, 5Kh6G1, 5D2	85	1150	140	250	420	49	1.9	4.5	19.4	21.8	18.2
7	ZhGr0, 5Kh6G1, 5MN4D7	65	1100	135	300	560	80	3.05	5.25	18.3	18.9	18.9
8	ZhGr0, 5Kh6N4D2	50	1100	-	-	-	-	-	-	-	-	-
9	ZhGr1, 5N4D7	75	1200	360	360	1090	44	6.4	4.8	14.3	15.2	16.1
10	ZhGr1, 5G1, 5MN4D2	85	1200	410	330	980	55	5.15	4.6	18.3	18.7	19.2
11	ZhGr0, 5G1, 5D7	65	1200	190	660	650	74	3.35	8.2	14.4	15.6	14.3
12	ZhGr0, 5MD2	50	1200	145	530	605	176	2.95	4.1	16.2	17.4	15.6
13	ZhGr1, 5G1, 5D7	50	1100	160	550	604	101	2.55	4.25	14.3	16.1	16.5
14	ZhGr1, 5MD2	65	1100	210	480	1070	56	2.55	6.5	14.3	15.83	15.9
15	ZhGr0, 5N4D7	85	1150	270	835	1447	48	6.15	10.0	14.3	14.9	13.3
16	ZhGr0, 5G1, 5MN4D2	75	1150	240	575	1207	45	8.7	5.9	14.6	15.3	13.5

* σ_B is the tensile strength, σ_i is the bending strength, a_n is the impact strength, P is the load on the mating surface in the wear test, and τ is the wear test time.

The composite was produced by infiltrating a powder-steel carcass with a copper alloy. The sum total of mechanical and thermophysical properties was studied because there are no data concerning the interrelationship between the tool's useful life and individual properties of its material. Experimental design was employed, using the design prescribed by indicator 222211B//16,[1] for the purpose of optimizing the composition of the carcass material. Taking into account the large number of factors and the lack of sure criteria for the material's fitness, the problem was solved in two steps and the size of the experiment was limited to 16 tests.

The content of alloying elements, the powder carcass's porosity and the sintering temperature were varied. The experimental design matrix is presented in Table 1.

The chromium content varied over the range of 0 to 6 percent, the manganese of 0 to 1.5 percent, the molybdenum of 0 to 1 percent, the graphite of 0.5 to 1.5 percent, and the copper of 2 to 7 percent. The starting density of the compacts was 50, 65, 75, and 85 percent. The sintering temperature was 1100, 1150, and 1200°C.

Powders of type PZhRV-3 iron (GOST [All-Union State Standard] 9849-76), high alloy PKh - 30 - 2S (GOST 13084 - 73), type MPCh molybdenum (TU [Specifications] 48 - 19 - 69 - 73), type PMS-1 copper (GOST 4960 - 75), type PNK nickel (GOST 9722 - 78), type FMnS ferromanganese (GOST 4755 - 70), and type GK-2 graphite (GOST 4404 - 78) were used as starting materials.

The starting powders were mixed in a ball mixer for three hours with a ball-to-mixture ratio of 2:1. Specimens for study were obtained by compacting to the required density. Compacts having a density of 50 percent were made by sintering a powder freely poured into a container of the required shape. Sintering was performed for two hours in a protective reducing atmosphere of dissociated ammonia having a dew point of not higher than -40°C. Infiltration was performed in a conveyer furnace at 1150°C by the method of applying a copper-iron-alloy compact to sintered compacts of the porous carcass.

The tensile strength, bending strength, impact strength, and Brinell hardness were determined in order to assess the level of the material's properties. The coefficient of thermal expansion was calculated according to plots

taken from a Netch dilatometer at 400, 600, and 800°C. Wear tests were performed on an MT-2 friction machine by the dry friction method, using a mating surface of type 25KhGM steel under a load of 5 kg for 10 minutes and 10 kg for five minutes. The length of the crater—which was used as the measure of wear resistance—was determined on a tool microscope after testing.

Optimization parameters were not obtained in test 8 in the process of conducting the experiment, because of the origin of a compacting crack in the compacts that was probably associated with the intense reduction of chromium oxides and the burning away of graphite in the sintering process. In this connection, the results obtained were analyzed from the general standpoint of a regression analysis of the relationships of the output parameters of the material's properties.[2,3]

The experimental results in question are presented in Table 1. An analysis of the results obtained revealed the following.

Chromium and manganese exert a significant influence on the composite's strength properties, and manganese reduces its ultimate strength and impact strength. This apparently occurs because manganese does not dissolve completely in the sintering process and an inhomogeneous structure forms. The introduction of molybdenum makes it necessary to raise the sintering temperature higher than 1200°C in order for the molybdenum to dissolve completely in the iron matrix and to gain optimal properties. Nickel's influence on the material's properties is strengthened when the copper content in the porous compact of the carcass increases. Alloying the material simultaneously with carbon and chromium reduces the effect of carbon's influence on the material's toughness and its hardness, because carbon reacts with chromium in the sintering process and carbides form, as the result of which the carbon content in the iron matrix is lowered. Increasing the quantity of carbon added causes the coefficient of thermal expansion to become higher than that of cast iron. This is not to be tolerated, because the item works in conjunction with cast iron parts. Raising the copper content in the porous compact of the carcass causes the composite's impact strength to be lowered.

Studies of the microstructure of the materials as a whole confirmed the results of the factorial experiment and disclosed that the introduction of a large quantity of alloying elements results in the formation of an inhomogeneous structure (Figure 1, a and b). Chromium is dissolved incompletely in materials having a low carbon content. This probably occurs on account of an insufficient amount of carbon for reduction of the oxide film of PKh - 30 particles. Increasing the graphite content to 1.5 percent brings about complete dissolution of the chromium, but results in the formation of carbides that are distributed nonuniformly over the material's volume. A fairly homogeneous pearlitic structure is observed in high-carbon chrome-free materials (Figure 1, c) and a pearlitic-ferritic in low-carbon. A sorbitic structure with retained austenite is observed in composite materials alloyed with nickel, manganese, and molybdenum (Figure 1, d).

Caption: Figure 1. Microstructures of Materials [Figure not reproduced]

Combinations of levels of factors providing optimal values of the parameters studied were obtained, based on the studies conducted. The upper and lower levels are designed by + and -, respectively. And by 0 if the influence is insignificant. Combinations of levels of factors providing optimal values of the parameters studied are presented in Table 2.

Table 2. Optimal Combinations of Levels of Factors for Parameters Studied

Parameter	Level of factors							
	Cr	Mn	Mo	C	Cu	Ni	θ	T_{sp} [sintering]
σ_B, max	-	-	0	-	+	0	0	
σ_i, max	-	-	0	-	0	0	+	-
a_n, max	+	-	-	+	-	+	-	-
L, min	+	0	0	0	0	0	0	0
CTE, min	-	0	0	-	0	0	0	0

Service tests of items made from the materials studied showed that a glass-molding tool made from the materials alloyed with nickel, maximum copper and minimum carbon, as well as with chromium and molybdenum and maximum carbon, has the longest life.

Conclusions

1. Relationships linking optimization parameters with varied factors, as well as with their interplay, have been established and analyzed, based on a regression analysis of the relationships of the output parameters of the material's properties. It was revealed that alloying with manganese is not to the purpose, because it has practically no influence on the material's strength properties.

2. The results of service tests of items made from the composites studied showed that a glass-molding tool's fitness for the task depends to the greatest extent on the impact strength, wear resistance, and ultimate strength of the material of which it is made.

Bibliography

1. Nelimov, V. V., editor, "Tablitsy planov eksperimentov dlya faktornykh i polinominalnykh modeley: Spravochnik" [Experimental Design Tables for Factor and Polynomial Models: Handbook], Moscow, 1982.

2. Solmen, R., "Sovremennaya metallurgiya" [Metallurgy Today], Moscow, 1970.

3. Drayner, N. and Smit, G., "Prikladnoy regressionnyy analiz" [Applied Regression Analysis], Book 2, Moscow, 1987.

Technological Possibilities for Use of Cold Forging of Iron Powder Blanks

917D0016A Moscow
KUZECHNO-SHTAMPOVOCHNOYE
PROIZVODSTVO in Russian No 5, 1990 p 10-12

[Article by Yu. A. Bobrovnik and I. S. Litmanovich: "Technological Possibilities for the Use of Cold Forging of Iron Powder Blanks"]

UDC 621.762.043.001.84

[Text] To study the possibility of using sprayed iron powder to produce parts with a density close to that of compact iron, we investigated the behavior of powdered iron materials in cold deformation processes and the physicomechanical properties achieved in them.

We studied PZhRV3.200.28 sprayed iron powder produced at the Brovarsk Powder Metallurgy Plant. We selected this kind of powder because of the conclusions of authors (National Powder Metallurgy Conference Proceedings, Boston, 1974. Princeton, 1974, No 7, pp 157-167) who claim that water-sprayed powders have a more successful set of properties suitable for the manufacture of high-density parts by cold forging powder blanks.

During cold closed upsetting of sintered iron powd we studied the compactibility of blanks with constant mass during upsetting in a closed press tool as a function of their original porosity, shape (degree of transverse deformation), and amount of compressed force.

The blanks' original porosity was set at 10 to 30 percent , the most common in manufacturing powder metal parts.

Forging pressures were set at 800 - 1200 MPa. The use of pressures below 800 MPa was ineffective from the standpoint of increasing blank density, while the use of pressures above 1200 MPa is restricted by the low durability of tools in quantity production.

Cylindrical specimens of the same mass were pressed from a charge that was a mixture of sprayed iron powder, to which 0.75 percent (by weight) zinc stearate had been added as a lubricant. A PMM - 125 hydraulic press was used for double-ended pressing, which ensures more uniform distribution of density through the body of the specimen.

The specimens were sintered in an OKB - 210A industrial pusher furnace in a protective endogas atmosphere under the usual iron sintering conditions, i.e., at 1150°C for two hr.

The specimens were sprinkled with calcined alumina to ensure uniform heating and to keep the specimens from swelling.

After sintering the alumina was cleaned off the specimens by vibrotumbling in dry sawdust, after which they were wiped off with a cloth.

Sintered specimens with different diameters and a specific porosity were upset on a PMM - 125 hydraulic press in a closed press tool to final diameter at pressures of 800, 1000, and 1200 MPa.

To reduce contact friction forces between the blank and the press tool's working surfaces, a layer of lubricant (molybdenum disulfide) was applied to the specimens by tumbling in a 1-liter double-cone mixer together with molybdenum disulfide powder and 8 x 8 x 8 mm porolon blocks.

When the specimen is set in the die, it had to be strictly arranged along the mold's center line to ensure uniform radial clearance.

The results of measurements of the forged specimens were used to determine the density, porosity, and degree of transverse deformation.

Analysis of experiment data shows an increase in the compactibility of powder blanks with an initial porosity below 25 percent if the metal freely flows transversely during upsetting in a closed press tool. This effect is most evident when the degree of transverse (lateral) deformation is $O<\varepsilon_L\leq 2.5$ percent (figure 1).

If transverse deformation is above 2.5 percent the effect of lateral metal flow on sintered powder blank compactibility is less evident. For example, if transverse deformation increases from 2.5 to 10 percent , porosity declines only 0.2 percent .

If the powdered blanks' initial porosity is above 25 percent , transverse deformation has almost no effect on compactibility. If initial porosity is above 30 percent , there is even a slight decrease in compactibility, which apparently results from the relative increase in the degree to which the material is work hardened and from the deterioration in its deformability as the blanks' initial porosity increases.

Comparing experimental data on the compactibility of powdered blanks with different porosities, we found that blanks with the minimum possible initial porosity must be used to achieve maximum density in forged parts. For example, at an upsetting pressure of 1200 MPa (cf. figure 1) specimens with an initial porosity of 30 and 10 percent are compacted to a residual porosity of 4.3 and 1.8 percent .

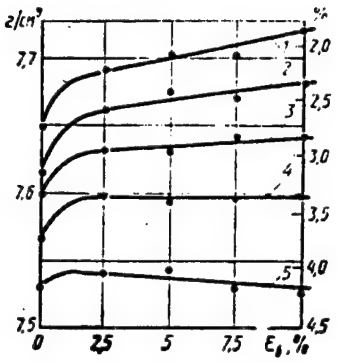

Figure 1. Sintered iron powder compactibility during forging in a closed press tool as a function of transverse deformation at 1200 MPa: 1, 2, 3, 4, 5 - initial porosity of 10, 15, 20, 25, 30%.

The curves in figure 2 show that the forged parts' density increases as upsetting pressure rises and as initial porosity drops.

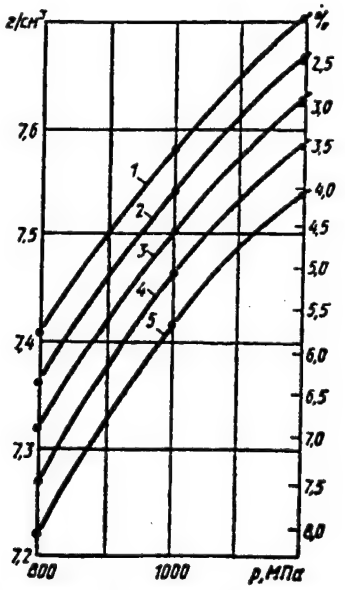

Figure 2. Sintered iron powder compactibility during forging in a closed press tool as a function of applied force (degree of transverse deformation ε_L = 5%): 1, 2, 3, 4, 5 - cf. figure

When we studied the process of direct extrusion of sintered iron powder, we investigated powder blank compaction as a function of initial porosity and of the degree of transverse deformation. We produced cylindrical specimens 18 mm in diameter and 20 mm high with different porosities from 10 to 30 percent similar to those used to study closed upsetting.

We adjusted the degree of deformation by changing the size of the die aperture and set it at 10 - 60 percent . We performed cold direct extrusion experiments on a 500 - kH P - 50 hydraulic press.

Analysis of the experimental data revealed that the density of the powder blanks increases as initial porosity decreases and as the degree of transverse deformation rises. However, the density at the stem portion of the forged part begins to decline, starting at a transverse deformation of 50 percent , regardless of initial porosity. This is because if the degree of transverse deformation is high, the diffusion bonds among the powder particles in a sintered porous blank rupture, which leads to a reduction in density in the stem portion of the part.

In addition, density is unevenly distributed in a forged part. It is always higher in the stem, where ductile flow takes place along with compaction, than in the head.

Specific forging force in direct extrusion of iron powder blanks is almost independent of initial porosity, while it increases linearly as the degree of transverse deformation rises.

As the results of the experiments show, circular cracks develop when iron powder blanks with an initial porosity above 10 percent and a transverse deformation above 40 percent are extruded. If transverse deformation exceeds 40 percent , cross-cut end cracks appear. The number and depth of circular and cross-cut end cracks increases with initial porosity.

Circular cracks apparently form because compressive stress constituents do not develop adequately during cold deformation. In this state, low density and the presence of a multitude of pores facilitate crack formation. Cross-cut end cracks also develop due to tensile stresses caused by the uneven flow of exterior and internal metal layers.

Hydraulic lift was used to eliminate cracks. Its use during direct iron powder blank extrusion has a positive effect on part quality: circular and cross-cut end cracks disappear regardless of initial porosities and degrees of deformation; density is more evenly distributed over the cross section of the forged parts; and final density becomes almost independent of initial porosity.

The lift force required to eliminate cracks increases with initial porosity when the degree of deformation is fixed. On the other hand, the required lift force declines monotonically when the deformation rises to 50 percent , but it begins to increase when deformation exceeds 50 percent .

The maximum density achieved in the stem end of a part was 7.74 g/cm$_3$ (residual porosity 3.1 percent).

Mechanical properties in tension were determined as per GOST 1497 - 84 on cold deformed specimens with a shape and size as per GOST 18227 - 85.

We produced blanks of the same mass with a porosity of 10 to 25 percent and different geometric dimensions to make the test specimens. The specimens were manufacture by cold upsetting blanks in a closed press tool.

When blanks with different cross sections were deformed in a press tool, the degree of transverse deformation was preset at 0 - 20 percent . The configuration of the press tool's working cavity ensured that specimens with a shape and size complying with GOST 18227 - 85 would be produced. Because of the specimens' complex shape, we used hydrostatic method (GOST 18898 - 73) to determine porosity.

During the experiments we studied the relationship of ultimate resistance and relative elongation to the specimens' initial porosity and degree of transverse deformation.

To determine the effect of post-forging heat treatment on mechanical properties, some specimens were annealed at different temperatures.

Annealing at 1150°C was done under sintering conditions in a protective endogas atmosphere.

Annealing at 750 and 350°C was done in a vacuum furnace at 0.13 Pa for 2 hr. Specimens were cooled to ambient temperature together with the furnace.

The experimental data make it possible to conclude that the relationship of ultimate resistance and relative elongation on the degree of transverse deformation is extreme (figures 3 and 4).

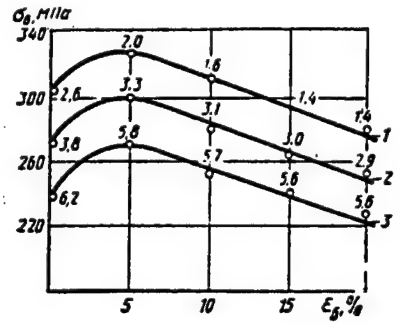

Figure 3. Ultimate resistance as a function of the degree of transverse deformation of blanks with 15% porosity: 1, 2, 3 - p = 1200, 1000, 800 MPa (numbers on the curves represent residual specimen porosity, %)

Maximum ultimate resistances and relative elongations occur at a transverse deformation of E_L = 5 percent .

If transverse deformation exceeds 5 percent , mechanical properties decline regardless of the fact that density continues to increase.

If transverse deformation remains the same, a reduction in the blanks' initial porosity lowers mechanical properties

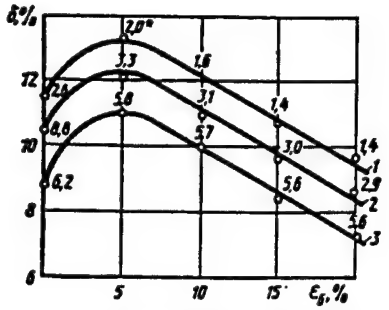

Figure 4. Relative elongation as a function of the degree of transverse deformation of blanks with 15% porosity: 1, 2, 3 - cf. figure 3

Heat treating cold-deformed iron increases ductility and slightly reduces strength. Low tempering (t≤350°C) has no noticeable effect on the specimens' mechanical properties. Annealing at t = 1150°C is optimum from the standpoint of achieving a set of high strength and ductility properties. The use of these annealing conditions made it possible to more than double the ductility of sintered cold deformed specimens during the experiment (figure 5), while the high level of strength remained unchanged (figure 6).

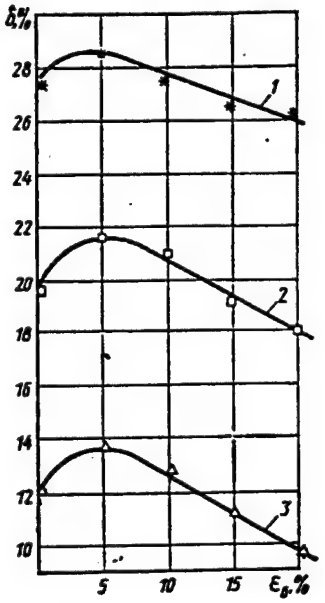

Figure 5. Relative elongation as a function of the degree of transverse deformation of blanks with 15% porosity annealed after deformation: 1, 2, 3 - t_{ann} = 1150, 750, 350°C

The method most structurally sensitive, impact strength testing, provides a picture of the structure of sintered material (pore shape, quality of metal contact between particles) and the proper selection of process conditions.

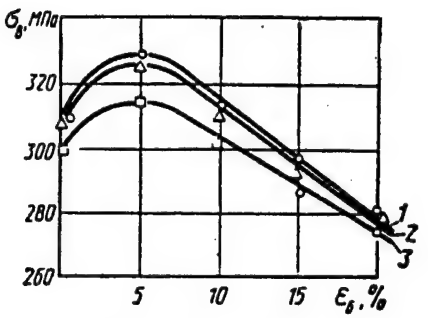

Figure 6. Ultimate resistance as a function of the degree of transverse deformation of blanks with 15% porosity annealed after deformation: 1, 2, 3 - cf. figure 5

This characteristic plays a major role in evaluating material quality, since the transition from static to impact loads, i.e., when loading rate increases significantly, causes a change in these properties, which are related to plastic deformation.

Mechanical properties during impact strength tests were determined on cold deformed specimens (GOST 26528-85).

Test specimens were produced just as those for tensile tests.

As in the previous case, the relationship of impact strength to the degree of transverse deformation is extreme, and the maximum impact strength occurs at 5 percent deformation.

If deformation remains the same, a decrease in initial porosity results in an increase in impact strength.

Analysis of the experiment results showed that heating treating cold deformed iron has a major effect on the iron's impact strength. The higher the treatment temperature, the greater the effect.

For example, the impact strength of specimens with an initial porosity of 15 percent with 5 percent deformation increases from 21 to 164 J/cm^2 as a result of annealing at t = 1150°C.

Heat treating these specimens at t = 350°C produces almost no change in their properties: impact strength increases only to 21.3 J/cm^2.

The studies thus showed that cold forging iron powder blanks makes it possible to produce structural products with a porosity to 1.4 percent . Powder products produced by cold cubic deformation have mechanical properties that differ little from those of products made of compact materials of similar composition.

Optimal Drawing Angles for Hardening Metal

907D0188C Moscow IZVESTIYA VYSSHIKH UCHEBNYKH ZAVEDENIY: CHERNAYA METALLURGIYA in Russian No 4, Apr 90 pp 27-29

[Article by Yu. S. Zykov, Zaporozhye Industrial Institute]

UDC 621.778

[Abstract] A study is made of the process of drawing a circular shape of a hardening metal in repeated drawing of wire initially through the first draw die with conical profile. It is found that with repeated drawing as the degree of preliminary hardening increases and the drawing factor per pass decreases the optimal angle somewhat decreases. This is significant only for the first one or two passes, however. An equation is derived to determine the drawing stress of a circular shape and compute optimal drawing angles considering the degree of hardening of the metal. Figures 2, references 8: Russian.

The Effect of Crystallization on the Structure of Alloys in the Fe - W System

917D0057D Moscow METALLOVEDENIYE I TERMICHESKAYA OBRABOTKA METALLOV in Russian Sep 90 pp 34-36

[Article by A.P. Gulyayev, O.D. Sidorova and T.P. Moskvina, Ferrous Metallurgy SRI imeni I.P. Bardin (Central)]

UDC 621.762:669.15'27:620.184

[Abstract] The structure and phase composition of 30 to 50 percent tungsten alloys obtained by granular metallurgy and the effect of crystallization rate on alloy structure are investigated. It was found that a maximal rate of cooling (more than 10^5 °C/s) by spraying during crystallization suppresses precipitation from the μ-phase (Fe_7W_6) in the liquid melt in 42 percent tungsten alloys. This high rate of crystallization facilitated complete dissolving of the tungsten (42 percent) into the solid solution of the alloy granules. Subsequent heating caused precipitation of the μ-phase in dispersed form. References 2 Russian; figures 4; tables 2.

Wear Resistance of Nitrided Powdered Mateials

917D0057E Moscow METALLOVEDENIYE I TERMICHESKAYA OBRABOTKA METALLOV in Russian Sep 90 pp 36-37

[Article by V.N. Glushchenko, L.P. Dmitriyeva and Ye.I. Frumkin, NIIAvtoprom NPO]

UDC 620.178.16:621.762:621.785.532

[Abstract] Powdered materials commonly used in machine building (iron-dusted powders PZhRP2.200.26

with graphite and copper additive, and inhomogeneously-Fe-doped powders of the Ultrapak variety) were compacted with an ultimate pressure of from 5 to 7 t/cm^2 and baked at 1120 - 1150 °C for 30 to 45 min, attaining a density of 80 to 90 percent. The samples were oxidized in air at 560 - 570 °C for 1 to 3 h, then nitrided at 570 °C for 5 h in a 50/50 mix of ammonium and natural gas. It was found that the 5 to 7 micron carbon-nitrogen layer thus formed increased the hardness from 150 to 350 HV and increased the wear resistance by a factor of 10 over untreated samples. However, strength and impact resistance were reduced, especially for materials with less than 90 percent density. Oxidation prior to nitriding localizes the nitrogen diffusion to the surface layer (a diffusion layer of less than 0.25 - 3.0 microns in a carbon-nitrogen layer 10 to 14 microns thick for 90 percent density ZhD2.5 powder), thus restoring these mechanical properties to their former levels. Figures 2; tables 1.

Fractographic Analysis of the Quality of Splicing in Carbon Steels

917D0057F Moscow METALLOVEDENIYE I TERMICHESKAYA OBRABOTKA METALLOV in Russian Sep 90 pp 38-40

[Article by Yu.G. Dorofeyev, Yu.V. Dybov, S.N. Yegorov, and Ye.I Kolokolov, Novocherkassk Polytechnic Institute]

UDC 621.762.4.04:621.78.061:669.14

[Abstract] The authors investigate the processes of splicing, i.e. solid phase formation of metal bonds at particle contact surfaces in powdered materials. Bushings were pressed out of cylindrical blanks at austenitic temperatures from steel with carbon content varying between 0.2 and 1.0 percent and welded together. Fractographic analysis of welded joints indicates that when tension is applied cracks are generated on weld defects (micropores, nonmetallic inclusions) and in regions of secondary phase precipitation—the "white streaks" at the layer interfaces. The quality of such splices is estimated from the bifurcation of the meshes appearing at intergrain laminations in the splice region. The existence of spallation regions in the splice region is characteristic of structures with small secondary phase seams; intergrain failures rather than intergrain failures would be indicative of higher weld quality. Increasing the rate of post-deformation cooling reduces the dimensions of the secondary phase, but also has a negative effect on mechanical failure properties. References 1 Russian; figures 4.

Critical Crystallization Rates for Tungsten Alloy Single Crystals

917D0050A Moscow IZVESTIYA AKADEMII NAUK SSR: SERIYA METALLY in Russian Sep-Oct 90 pp 66-71

[Article by S.N. Dubinin, V.N. Zagryazkin, and V.A. Repiy, Moscow]

UDC 669-669.27:548.55

[Abstract] A comparison is made of the critical crystallization rates (the rate for which defects and instabilities begin to occur in the plane front) calculated by the concentration supercooling criterion, Kurz - Fisher criterion or Mullins-Sekerka criterion for W - Nb, W - Re and W - Ta alloys. It is shown that these estimates do not differ significantly in the 0 to 10 percent alloy concentration range. One advantage of the Kurz - Fisher method is that it lets us determine the range of crystallization rates corresponding to evolution of a crystallization front from plane to dendritic morphology. In addition, comparing experimentally-determined rates for crystallization corresponding to the transition to polycrystalline growth with the ranges calculated from the Kurz-Fisher criterion enables us to estimate the temperature gradient in the liquid phase, which is roughly 1000 to 1100 K/cm for a plasma arc melt and 500 to 700 K/cm for an electron beam melt. References 15: 8 Russian, 7 Western; figures 3; tables 3.

Characteristics of Ferrite Recrystallization in Cold-Rolled Low- Carbon Steel

917D0050B Moscow IZVESTIYA AKADEMII NAUK SSR: SERIYA METALLY in Russian Sep-Oct 90 pp 98-99

[Article by V.I. Movchan, N.A. Grudeva, N.V. Podobedova, V.F. Martsiniv, and E.N. Mikhaylenko, Dnepropetrovsk]

UDC 669.017.3:548.53

[Abstract] The recrystallization of ferrite was studied in type 08 cold-rolled low-carbon steel relatively free of cold defects (by mass percent, C 0.07, Mn 0.27, Si 0.01, S 0.026, P 0.009, Ni 0.08). The samples were heated to 800 |SDC, at which point the second phase of austenite regions appeared, then the samples were held at 400 |SDC for 1 h and etched to reveal the ferrite fine structure. More than 80 percent of the matrix was made up of polygonal-structure grains. It was found that even relatively large inclusions can hold back recrystallization by halting the migration of grain boundaries, particularly if the driving force of the process is reduced by prior formation of polygonal structures. References 6: 3 Russian, 3 Western; figures 1.

The Form and Structure of Nickel-Based Rapidly-Solidified Powders

917D0046A Kiev POROSHKOVAYA METALLURGIYA in Russian Aug 90 pp 1-5

[Article by A.A. Ivlev, L.A. Gorbatenko, V.I. Kalita, V.V. Kudinov, and B.K. Vernikovskiy, Tulachermet NPO and USSR Academy of Sciences Metallurgy Institute]

UDC 669.017:621.767:539.213

[Abstract] The cooling rate in gas-deposited PG - SR4 powder using traditional methods is too low for formation of an amorphous state, despite the presence of amorphous elements (Ni base, 16 to 18 mass percent Cr, 3.8 to 4.5 percent Si, 3.1 to 4.0 percent B, 0.8 to 1.2 percent C, and up to 5 mass percent Fe). Rapid solidification is accomplished by depositing the powder from a high-energy gas flux onto a copper water-cooled recrystallizer surface, and the authors used X-ray diffraction and metallographic methods to study six different fractions of the powder to determine the effect of this increased cooling on its phase content, morphological and structural parameters. In the under-63 micron fractions, spherical or nearly spherical morphology dominates, but flaky particles become more common as the fractions increase up to 315 microns. An amorphous phase may be obtained from these flaky particles under conditions that maximize the cooling rate, i.e., minimum flake thickness and maximum surface contact area of a drop of alloy after it strikes the recrystallizer. References 2 Russian; figures 3; tables 1.

Behavior of Powder Particles Bonding Under Plastic Deformation

917D0046B Kiev POROSHKOVAYA METALLURGIYA in Russian Aug 90 pp 15-20

[Article by V.A. Arefyev, V.V. Kuleshov, and V.M. Panovko, USSR Academy of Sciences Metallurgy Institute]

UDC 621.762

[Abstract] This article checks on the theoretical prediction that the strength of the bonds holding a powder compact together after plastic extrusion is proportional to the specific renewed surface area of the particles, i.e., the new surface formed as the particle undergoes plastic deformation. Plotting the bond strengths of various fractions as a function of specific renewed surface, deformational and dimensional components of the specific renewed surface, and contact surface at 400 |SDC of extruded spherical aluminum powder shows that it is indeed dependent on the specific renewed surface alone under mechanical activation, and independent of the method in which that renewed surface was obtained. A downward shift of the curve at lower compacting temperatures is associated with the interactions of the contact surfaces via active centers that reduce the gripping surface relative to the renewed surface. The dimensions of the active centers determined in this experiment agree with those in the literature. References 6: 5 Russian, 1 Western; figures 4; tables 1.

Manufacturing Conditions of Rapidly-Quenched Ribbons of Fe-6.5 Percent Si Alloys Affecting Its Structure and Magnetic Properties

917D0046B Kiev POROSHKOVAYA METALLURGIYA in Russian Aug 90 pp 30-35

[Article by V.Z. Balan, V.V. Maslov, V.K. Nosenko and D.Yu. Paderno, USSR Academy of Sciences Metallurgy Institute]

UDC 621.762

[Abstract] Rapidly-solidified ribbons were made from especially pure Fe - 6.5 percent Si alloys in air on copper and steel chillblocks, and in a carbon dioxide atmosphere on steel chillblock. The quality of the ribbon (surface finish, gas inclusions, etc.), plasticity as a function of ribbon thickness, and magnetic properties (magnetic field strengths, specific hysteresis losses and magnetic susceptibility at 1100 - 1200 |SDC) were determined for each process. It was found that processing in the carbon-dioxide atmosphere significantly improved the surface finish on all sides of the ribbon. The dispersion and uniformity of the ribbon microstructure was found to depend on the strength of adhesion between chillblock and ribbon, which in turn depends on the area and duration of contact. Forced cooling of ribbons thicker than 40 microns following release from the chillblock was found to improve their plasticity. The improved quality of ribbon surfaces from rapid solidification in a carbon dioxide atmosphere was accompanied by better magnetic properties. References 8: 4 Russian, 4 Western; figures 3; tables 2.

Microhardness of Amorphous Metal Alloys of Fe-Cr-B

917D0046D Kiev POROSHKOVAYA METALLURGIYA in Russian Aug 90 pp 49-53

[Article by Yu.V. Milman, S.V. Pan, S.V. Postoy, and R.K. Ivanshchenko, UkSSR Academy of Sciences Problems of Materials Science Institute]

UDC 539.213:669.12'5:669.26:669.781:539.533

[Abstract] Results are presented of a systematic study of the microhardness of the amorphous metallic alloys $Fe_{83}B_{17}$, $Fe_{80}Cr_5B_{15}$, $Fe_{75}Cr_{10}B_{15}$, and $Fe_{70}Cr_{15}B_{15}$ in the 77 - 873 K temperature range, and of the influence of chromium content on the Vickers hardness as a function of temperature for these alloys. The alloys were formed into 20 to 30 micron thick ribbons by melt spinning onto a chillblock, with a cooling rate of 10^6 |SDC/s. The hardness was determined using a diamond-tipped indenter under 1.8 N load; the mean-square deviation of the HV values from the average was less than 5 percent. Four temperature regions may be discerned: less than 200 K—HV is the sum of two components, one governed by metalloid content, and the other by the number of metal elements; between 200 and $0.7T_{cryst}$, where only

metalloid content has any effect; between $0.7T_{cryst}$ and T_{cryst} (about 700 K) where there is a switch from a nonhomogeneous to homogeneous plastic deformation mechanism and an inflection point in HV(T); and greater than T_{cryst}, where there is a sharp peak in HV associated with onset of the crystallization process. These results, particularly at low temperatures, indicate that these amorphous metallic alloys are intermediate between metals and covalent crystals. References 11: 8 Russian, 3 Western; figures 4; tables 1.

Tribological Properties of Nonmetallic-Nitride-Based Ceramic Alloys I. Frictional Characteristics of Aluminum Nitride-Based Composite Materials

917D0046E Kiev POROSHKOVAYA METALLURGIYA in Russian Aug 90 pp 76-80

[Article by A.D. Pansyuk, L.I. Struk, A.I. Yuga, L.F. Kolesnichenko, I.P. Neshpor, and O.I. Fushchich, UkSSR Academy of Sciences Problems of Materials Science Institute]

UDC 539.621:666.3/7

[Abstract] This article studies the tribological properties of AlN, AlN-Si_3N_4, AlN-BN and AlN-TiN ceramic alloy composites in a frictional pair with heat-treated grade 45 steel. Measurements of linear wear of the frictional surfaces and coefficient of friction were made on an MT - 68 friction machine (shaft/bushing type) at speeds between 4 and 16 m/s, and loads from 0.5 to 2 MPa. The AlN - BN system has the highest coefficient of friction (0.35 to 0.40) and wear (10 to 40 microns/km). AlN - Si_3N_4 friction was found to depend essentially on the porosity of the sample. Formation of Al_2O_3 and TiO_2 oxides on the surfaces of the AlN - TiN acted as a solid lubricant, giving this alloy the lowest friction and wear of those tested and increasing its hardness. References 7: 5 Russian, 2 Western; figures 6.

Properties of Powder Alloyed Structural Steels Manufactured Under Experimental Industrial Conditions

917D0046F Kiev POROSHKOVAYA METALLURGIYA in Russian Aug 90 pp 96-100

[Article by V.N. Klimenko, S.G. Napara-Volgina, T.A. Guller, A.K. Gayduchenko, V.D. Pirog, L.M. Klevtsova, and V.V. Mizyuk, UkSSR Academy of Sciences Problems of Materials Science Institute]

UDC 621.762

[Abstract] An investigation is made of the effect of porosity, bound carbon content, alloying and manufacturing technique on the properties of powder-alloyed materials made by compaction (700 - 800 MPa) and sintering (1050 - 1200 |SDC) at the pilot Brovary Powdered Metals Plant. The alloys contained between two and 10 percent Cu, Cu + Ni, Ni + Mo or Ni + Mo + Cu, and carbon content varied from 0.02 to 1.25 percent. Bound carbon content and degree of alloying were found to have a most significant influence on mechanical properties; 0.5 to 0.6 percent carbon content was found to be optimal in the Cu and Cu + Ni alloys. For identical carbon content, the highest degree of homogeneity was found in the partially alloyed powders. References 6 Russian; figures 4; tables 1.

Tribological Characteristics of Glass Ceramic/Steel 45 Friction Pairs

917D0046G Kiev POROSHKOVAYA METALLURGIYA in Russian Aug 90 pp 100-103

[Article by A.I. Yuga, V.D. Derkach, T.M. Chevychelova, N.D. Nazarenko, and G.g. Kardyuk, UkSSR Academy of Sciences Problems of Materials Science Institute]

UDC 666.266.(088.8)

[Abstract] The authors have evaluated the effect of diffusion borating a hardened grade 45 steel shaft on its coefficient of friction and linear wear when paired with a glass ceramic bearing. Two bearing materials were tested: Sitall and Sitall plus 30 mass-percent copper fractions of less than 60 microns. Measurements were made on an MT - 68 friction machine at speeds ranging from 5.0 to 15.0 m/s and pressures from 2.5 to 5.0 MPa. The Sitall and hardened steel 45 pair showed a slightly less friction and wear as the speeds increased, due to the oxide coating formed at the higher temperatures, but both it and the Sitall/borated steel 45 pair failed at 10 to 12.5 m/s. By contrast, in the Sitall + Cu/borated steel 45 pair the coefficient of friction varied from 0.08 to 0.10, and wear remained at less than 25 microns/km at 10 m/s. References 5 Russian; figures 2; tables 1.

Using Microscopic Arc Oxidation To Make Dielectric Coatings on Aluminum and Aluminum Alloy Parts

917D0043A Kishinev ELEKTRONNAYA OBRABOTKA MATERIALOV in Russian May-Jun 90 pp 20-22

[Article by A.P. Brynzan, Ch.T. Kantser, and V.A. Kaplin, SKTBTE of the Moldavian SSR Academy of Sciences Applied Physics Institute]

UDC 621.357.8(088)

[Abstract] AMG-3, AMTs and D16AT aluminum alloys were oxidized in sodium hexametaphosphate electrolyte in an arc discharge of 350 to 500 V and 5 to 10 A/dm^2. The coating was 20 to 30 microns thick, adhesive strength was more than 200 kgf/cm^2, surface finish of 0.8 to 1.0 microns, breakdown voltage 350 to 400 V, and heat conductivity 1.5 to 2 W/cm.deg. X-ray phase analysis of the coating using a DRON-2 diffractometer on CuK_α-emissions revealed diffraction lines belonging to α - Al_2O_3 - corundum. Electron microscope investigation (x 10,000) reveals nonuniform distribution of irregularly shaped "islands" less than 20 microns long separated by cracks 0.1 to 1 microns wide. Increasing the discharge voltage seems to decrease the number of pores per unit surface area. Tests of parts coated in this manner in use on plasma- chemical etching devices demonstrates superior corrosion resistance properties resulting in ten times the normal service life of the equipment. References 4 Russian; figures 2.

On the Question of Mass Transfer in Vacuum Electric Arc Deposition of Multicomponent Coatings

917D0043B Kishinev ELEKTRONNAYA OBRABOTKA MATERIALOV in Russian May-Jun 90 pp 22-24

[Article by B.A. Eyzner, Belorussian SSR Academy of Sciences Physical Technical Institute, Minsk]

UDC 621.793.1

[Abstract] The surface of a vacuum arc deposited multicomponent coating is characterized by the formation of peaks and valleys, unlike that of electron beam vacuum evaporation coatings. This is due to the fact that lighter, high-charge ions will be deflected more than heavier, less charged ions in the neighborhood of surface irregularities that alter the accelerating field between cathode and substrate. The heavier, less-charged ions build up as peaks, further altering the electric field in their vicinity and continuing the peak- formation process. This structure has been observed in NiCrAlY, CoCrAlY and TiSi multicomponent coatings. A test was conducted which confirmed the prediction that the difference in chemical element composition between cathode and coating would increase as displacement potential increased, and hence intensity of peak formation and self- sputtering increased. References 3 Russian; figures 2.

Effect of a Pulsed Magnetic Field on the Discharge Channel-Electrode Surface Interaction

917D0043C Kishinev ELEKTRONNAYA OBRABOTKA MATERIALOV in Russian May-Jun 90 pp 24-26

[Article by A.Ye. Gitlevich, A.N. Vishnevskiy, and P.A. Topala, Moldavian SSR Academy of Sciences Applied Physics Institute, Kishinev]

UDC 537.521:621.9.048.4

[Abstract] Flat steel St3, titanium VT23 and copper M1 electrodes were subjected to pulsed discharges of 1.0 to 1.7 kA at 160, 240, 320 and 400 V with a pulse width of 200 microseconds and prf of 10 to 15 Hz over a gap of only 0.5 to 1.5 mm, with a transverse pulsed magnetic field applied. A decrease in the size of the electrode spot was noted when the magnetic field was applied, and this effect was intensified the larger the interelectrode gap. The field also lengthened the erosion trail on the electrode in the magnetic force direction. An increased electrode temperature in the interaction region of the magnetic field and discharge plasma results in predominantly liquid phase there. References 9 Russian; figures 3.

Laser Heat-Treatment Hardening and Increasing of Surface Wear-Resistance of Steel 9KhF

907D0175A Minsk TRENIYE I IZNOS in Russian No 3, May-Jun 90 pp 435-440

[Article by G.I. Kozlov and A.D. Sokurenko, Institute for Mechanics Problems, USSR Academy of Sciences, Moscow]

UDC 621.048.7

[Abstract] Specimens of steel 9KhF were scanned with a 10-kW CO_2 laser focused with an NaCl lens to produce a hot spot from 2 to 5 mm in diameter. The energy density on the specimen surface was varied from 4000 to 32000 W/cm^2. The exposure time was varied from 0.005 to 0.8 s. The specimen surface was protected with helium and with soot. Microhardness measurements show that short exposure times produce a hardened path narrower than the hot-spot diameter. The hardened-path width increases with increasing exposure time, but this is accompanied by a smaller hardness increase because of reduced heat transfer to the areas adjacent to the hot spot. The depth of hardening increases with exposure time. The best combination of the depth of hardening and hardness (0.9 mm and 7000 Mpa) without melting the surface was obtained with energy density of 4000 W/cm^2 and exposure time of 0.4 s. Wear tests show that the rate of wear of untreated specimens is 57 times as

high as that of the outermost layer of the specimens hardened under the optimum conditions. The rate of wear of these hardened specimens increases slowly to the depth of about 0.5 mm and then grows rapidly. This is attributed to the fact that the hardened layer consists of hardened spots interspersed with nonhardened spots, and the number of the nonhardened spots increases with increasing depth. Figures 4; 2 Russian references.

Breakdown of Hard Coatings on Steel Under Contact Impact Loads

907D0175B Minsk TRENIYE I IZNOS in Russian No 3, May-Jun 90 pp 490-494

[Article by G.M. Sorokin, Yu.V. Kolesnikov, and Yu.V. Zhostik, Moscow Petroleum and Gas Institute and Bryansk Transport-Equipment Institute]

UDC 621.891:621.375.826

[Abstract] Silicon carbide coatings 0.2 mm thick with a surface microhardness of 25 GPa were applied on end faces of 12-mm diameter cylindrical specimens of steel 45 quenched and tempered to HRC 55, and the coatings were tested with a tungsten carbide indentor placed in contact with the coatings to simulate penetration of an abrasive particle into the coating. The indentor energy was varied by varying either the weight or the speed of the hammer used to hit the indentor. The tests resulted in an indentation, cracks radiating from the indentation, and arc-shaped cracks coaxial with the indentation. The rate of length increase of the radial cracks increases with the impact energy until the impact energy becomes sufficient to penetrate the entire coating thickness (1 J in the case of the indentor used). The spalling away of a coating segment requires approximately the same impact energy in the case of a single impact as the sum of impact energies in the case of smaller multiple impacts. It was found that the ratio of the average length of the radial cracks to the indentation diameter is a good measure of the abrasion resistance of the coatings. Figures 4; 11 Russian references.

Structure and Properties of Surface Layers of Iron-Silicon Alloys After Heat Treatment and Abrasive Wear

907D0175C Minsk TRENIYE I IZNOS in Russian No 3, May-Jun 90 pp 509-512

[Article by Ye.P. Yelsukov, V.V. Tarasov, Yu.I. Filippov, and G.N. Konygin, Physics Technology Institute, Ural Department, USSR Academy of Sciences, Izhevsk and Metal-Physics Institute, Ural Department, USSR Academy of Sciences, Sverdlovsk]

UDC 539.211:669.15.782

[Abstract] A study of the relationship between the wear resistance and structure and microhardness of surface layers of nonporous iron-silicon alloys after heat treatment and abrasive wear is reported. iron-silicon alloys containing up to 33 at. percent Si were heat treated to produce an ordered metastable DO_3 superlattice and subjected to wear with abrasive paper. The surface structure before and after abrasive wear was determined by Mossbauer conversion-electron spectroscopy and Mossbauer X-ray spectroscopy. It was found that abrasive wear leads to an unordered state of the surface layer to the depth of 10 microns. The microhardness of the surface layer increases with silicon content and by work-hardening in the course of abrasive wear. The wear resistance was found to increase with increasing microhardness of the alloys in the unordered condition. It is concluded that a 50 percent wear resistance increase can be obtained by increasing the silicon content of the iron surface from the usual 20 percent to about 33 percent. Figures 3; references 12: 10 Russian, 2 Western.

Antifriction and Continuity-Retention Properties of an Electrodeposited Superplastic Cd-Zn Coating in Plastic Deformation by Upsetting

907D0175D Minsk TRENIYE I IZNOS in Russian No 3, May-Jun 90 pp 513-515

[Article by N.P. Barykin and F.A. Sadykov, Metals Superplasticity Institute, USSR Academy of Sciences, Ufa]

UDC 621.7.029 : 669.735

[Abstract] The variation of the friction coefficient of a superplastic Cd - 17.5 percent Zn coating on ring specimens of Armco iron with temperature (20 and 150°C) and strain rate (10^{-3} to 10 s^{-1}), as well as the variation of the coating strain with the strain rate of coated cylindrical specimens (a measure of continuity retention) are reported. The friction coefficient in a 100 kN upsetting press drops from about 0.12 at a strain rate of 10^{-3} s^{-1} (at both test temperatures) to a minimum of about 0.08 at a strain rate of 10^{-1} s^{-1} at 20°C and about 0.06 at a strain rate of 10^{-2} s^{-1} at 150°C and then increases with increasing strain rate at both temperatures. The coating strain decreases slowly with the specimen strain rate between 10^{-4} s^{-1} and 10^{-2} s^{-1}, goes rapidly to a minimum at a strain rate of 10^{-1} s^{-1}, and then increases sharply. The friction-coefficient and coating-strain minima are close to the region of optimum conditions for superplastic behavior of the coating. Figures 4; references 7: 5 Russian, 2 Western.

Increase of Antifriction Properties of a Titanium Alloy By Chemical and Thermal Treatment in Molten Salts

907D0175E Minsk TRENIYE I IZNOS in Russian No 3, May-Jun 90 pp 516-520

[Article by P.Sh. Lantsman and N.S. Ananin, Kuybyshev]

UDC 621.758.5 : 669.295.018

[Abstract] Disc specimens of VT14 titanium alloy were oxidized at 853 K for up to 3 h in a molten-salt mixture consisting of lithium carbonate, sodium carbonate, and lithium fluoride. X-ray, metallographic, and electron-microscope studies showed that the resulting surface layer contained α - TiO, anatase, Ti_2O, Ti_2O_3, Ti_3O_5, and a small quantity of γ - Al_2O_3. Vibration-tribometer and wear tests show that the oxide layer reduces the sliding and static friction by about 50 percent, increases the wear resistance, and permits higher loads to be used without seizing. Oxide layers produced by air-oxidation at 973 K in a fluidized bed have similar antifriction properties in the vibration-tribometer tests, but their static-friction coefficient is twice as high as that of oxide layers produced in molten salts. Because they are harder, they tend to spall and act as abrasives. Figures 3; tables 2; references 11: 10 Russian, 1 Western.

Study of Tribological Properties of Wear-Resistant Coating Based on Modified SKN Elastomer

907D0175F Minsk TRENIYE I IZNOS in Russian No 3, May-Jun 90 pp 538-540

[Article by V.N. Drobyshevskiy and A.A. Ryskulov, Institute for Metal-Polymer Systems, Belorussian SSR Academy of Sciences, Gomel]

UDC 624.43-242

[Abstract] Tribological measurements show that addition of 50 percent of VDU resin (oligomer of dimethylvinylethynilphenol) to SKN butadienenitrile rubber produces dip coatings from acetone solution on polyamide 6 that are much more wear resistant and possess much higher antifriction properties in friction couples with steel 45 lubricated with water-oil emulsions than unmodified SKN coatings. Also, these properties increase with contact pressure in the case of the modified coatings. This is attributed to structure changes that occur during curing and operation of the coatings as well as to adsorption of oil from the lubricant and its release to the contact zone as the contact pressure increases. One figure; ten Russian references.

Hydroabrasive Wear of Copper-Based Composite Materials

907D0175G Minsk TRENIYE I IZNOS in Russian No 3, May-Jun 90 pp 541-543

[Article by V.N. Kuskov and I.D. Morgun, Tyumen Industrial Institute imeni Lenin's Komsomol]

UDC 620.178.16 : 621.762

[Abstract] Three cylindrical copper-alloy powder compacts dispersion-hardened with green silicon carbide were tested for abrasion resistance in a water-sand stream with the aim of using these materials as substitutes for a wear-resistant bronze for bushings in submerged oilfield pumps. The compositions of the materials (in percent) were as follows: 1) 61.6 Cu, 4.8 Ni, 8.8 Al, 4.8 Fe, 20 SiC; 2) 70.4 Cu, 0.8 Ni, 6.4 Al, 2.4 Fe, 20 SiC; and 3) 58.7 Cu, 16.6 Ti, 0.7 Ni, 5.3 Al, 2.0 Fe, 16.7 SiC. The first two materials are recommended as substitutes for bronze because of their low microhardness (0.8 - 1.0 and 1.7 - 4.0 GPa), high strength (70.5 and 65.2 MPa) and low wear rate (0.62 and 0.44 $g/m^2/h$, compared to 0.90 $g/m^2/h$ for bronze). The third material is not recommended because of its high microhardness (5.3 - 8.5 GPa), and consequently high brittleness, and its low strength (30.8 MPa), although its wear rate of 0.67 $g/m^2/h$ is not significantly higher than that of the first material. The high microhardness and brittleness of the third material is attributed to the formation of Ti - Cu intermetallic compounds during sintering. One table; two Russian references.

Structure Formation in High-Speed and High-Chromium Stamping Steels With Laser Heating

907D0188D Moscow IZVESTIYA VYSSHIKH UCHEBNYKH ZAVEDENIY: CHERNAYA METALLURGIYA in Russian No 4, Apr 90 pp 68-70

[Article by V. B. Babushkin, L. G. Voroshnin, V. S. Ivashko, and V. V. Parkhimovich, Belorussian Polytechnical Institute; Belorussian Republic Scientific-Production Association for Powder Metallurgy]

UDC 621.785.545

[Abstract] A study is made of the structure and phase transformations in high-speed and high-chromium stamping steels upon laser heating at 3 x 10^3 to 10^5 - 10^6°C/s without melting the surface. Studies were performed on specimens of type R6M5 high-speed steel and Kh12M stamping steel in the annealed, hardened and tempered states. The structure of the steels was studied by metallographic and X-ray analysis and examined on a scanning electron microscope. The quantity of residual austenite was determined. It was found that heating rates of 3 x 10^3°C/s and higher the primary carbides are not dissolved—there is practically no diffusion interaction of the carbides with the matrix up to the melting point. Secondary carbides are partially dissolved under these conditions in annealed steels. Laser treatment forms a structure consisting of martensite, primary and incompletely dissolved carbides. Laser heating without melting of the surface is not suitable for hardening of annealed high-speed and high-chromium stamping steels. The effect of laser heating without melting of the surface consists of an increase in the dispersion of the martensite. Figures 2, references 8: Russian.

Increase in Uniformity of Carburization of High-Chromium Steels

907D0188E Moscow IZVESTIYA VYSSHIKH UCHEBNYKH ZAVEDENIY: CHERNAYA METALLURGIYA in Russian No 4, Apr 90 pp 71-73

[Article by V. S. Popov, N. N. Brykov, M. I. Andrushenko, and I. V. Bryndin, Zaparozhye Machine-Building Institute]

UDC 669.15-26-194.155

[Abstract] It is known that during casehardening in a solid carburizer, carburization of the part occurs primarily through the gas phase, meaning that direct contact of carburizer grains with the casehardened surface is not necessary. Based on this, the possibility was studied of producing uniform carburized layers of high-chromium steel by case hardening without direct contact of the part and carburizer. It was assumed that separation of the carburizer from the part could decrease the degree of saturation of the casehardened surface with carbon and avoid the formation of a carbide crust, and also eliminate nonuniformity of carburization. Studies were performed on steels type 08Kh13, 12Kh13 and 20Kh13 in a standard charcoal carburizer with the addition of 10 to 15 percent calcined sodo or 8 to 10 percent sodium acetate at 950 to 1080°C, five to 14 hours. A uniform layer was formed on the surface with about the same total thickness as in contact methods. No carbide crust was formed. The wear resistance of parts was three to five times higher than that of standard type 20Kh casehardened steel. Figure 1, references 10: Russian.

Gas Laser Cutter

917D0079B Kishinev ELEKTRONNAYA OBRABOTKA MATERIALOV in Russian No 4, 1990 p 90

[Article "Gas Laser Cutter"]

[Text] The gas laser cutter is designed for the laser cutting of metals and nonmetals by means of pulsed and continuous-wave industrial high-light lasers and can be used in any sector of the national economy where the precision cutting of sheet and three-dimensional products is required.

The gas laser cutter operates in combination with laser production systems (LTK's) and in the continuous-wave mode achieves key process indicators at the following levels: surface roughnesses not higher than 2 to 6 μm for a cut in titanium alloys, and not higher than 10 to 15 μm in stainless and high-alloy steels with a cut width of 0.1 to 0.25 mm and a heat-affected area of not larger than 0.2 mm. The cutter's design calls for it to work with both crystal and mirror focusing optics.

The use of a gas laser cutter achieves the reduced consumption of process gas, the highly efficient use of laser radiation, high reliability, simplicity of design, low weight, and the expansion of production capabilities with regard to the range of parts that can be worked.

Technical Data

Process gas pressure, MPa	To 2.5
Gage pressure of process gas at focusing optics, MPa	Not greater than 0.02
Nozzle diameter, mm	0.4 to 2.0
Radiated power of laser, kW	0.1 to 100
Laser radiating aperture, degrees	2 to 30
Process gas saving, percent	To 50

The design features that have been implemented are patentable and incorporate know-how.

We are offering the following:

A manufacturing and know-how license.

A contract for the development of gas laser cutters for specific laser production equipment and systems.

Our address: 420111. g. Kazan, K. Marksa, 10, Kazan Aviation Institute, Patent Department, telephone: 39-71-98

Arc Burning and Metal Transfer in Underwater Welding With Self-Protected Powder Wire

917D0030A Kiev AVTOMATICHESKAYA SVARKA in Russian Jun 90 pp 1-4

[Article by I. K. Pokhodnya, V. N. Gorpenyuk, V. Ya. Kononenko, V. Ye. Ponomarev, and S. Yu. Maksimov, Institute of Electric Welding imeni Ye. O. Paton, Ukrainian Academy of Sciences]

UDC 621.791.75.048(204):621.3.014.31

[Abstract] In order to assure good quality welded joints and increase the productivity of welder-divers, welding materials are needed with good welding properties, which in turn requires reliable experimental data on the burning of the welding arc and transfer of melted metal under the conditions encountered in underwater welding. This article presents results obtained with a type ANP-2 unsteady process analyzer, which can measure the electrical and time parameters of the arc and provide information in statistically processed form on graphic and digital displays. Welding was performed by an automatic welding machine in a special high-pressure water-filled chamber using type PPS-AN1 wire and an experimental wire containing a small quantity of REM as a stabilizer. The pressure in the chamber was equivalent to the water pressure at depths of 0.5, 10, 20 and 50 m. Welding was also performed in air for comparative purposes. A type ASUM - 400 power supply was used, the arc voltage was held at 28 - 30 V, welding current 120 - 220 A, increasing with depth. The metal transfer was estimated based on the length and frequency of short circuits. The specifics of arc burning were analyzed by studying curves of the arc voltage and current by processing the multimodal distributions. The number of events in each section of the curve, mean values of parameters, variations and dispersions were determined for each section of the curve. These data allow complete evaluation of the arc process and the transfer of electrode metal through the arc gap without the use of high-speed motion pictures, which are difficult to make under water. The frequency of long short circuits increases with increasing water pressure, reducing the stability of the process. The short circuits occupy up to 24 percent of the total time when PPS-AN1 wire is used. The information required for a deeper understanding of the process of welding under water can be obtained by analyzing the voltage and current curves, presented with the article. The experimental wire is superior at all depths. The behavior of the arc and the nature of melting of the electrode metal under water differs significantly from the same characteristics in air. The water vapor which makes up the bubble in which the arc burns dissociates into hydrogen and oxygen, which influence the stability of arc burning and the transfer of the melted metal. Two types of short circuits are observed at great depths: 1) those caused by growth of a drop of electrode metals; and 2) those caused by brief contact between the end of the electrode wire and the surface of the bath. The fraction of short circuits of the second type increases with depth,

primarily due to a decrease in the dimensions of the gas bubble. The introduction of rare earth metals to the welding wire significantly increases the stability of the process, reducing the number and duration of interruptions in burning of the arc, significantly reducing the size of the transient drops and decreasing the variation in the distribution of voltage and current. Figures 6; References 2: Russian.

Structure and Mechanical Properties of 1420 Alloy Welded Joints Made by Electron-Beam Welding

917D0030B Kiev AVTOMATICHESKAYA SVARKA in Russian Jun 90 pp 16-19

[Article by I. Ye. Sklabinskaya, A. V. Lozovskaya, and N. G. Tretyak, Institute of Electric Welding imeni Ye. O. Paton, Ukrainian Academy of Sciences]

UDC [621.791.72.052:669.715.002.28]:620.17

[Abstract] When type of 1420 alloy is welded the porosity of the seam metal is the main factor determining the strength of the welded joints. The problem of eliminating porosity and improving the mechanical properties of welded joints has now been successfully solved by the use of a special technology for preparation of the metal before welding, by the use of new power supplies, and by heat treatment before and after welding. When thick pieces must be welded, the problem arises of the influence of structural homogeneity on the mechanical properties of the welded pieces and their joints. This article discusses the results of a comparative study of the structure, properties of sheets, plates and press strips, influence of the structure of the initial metal on the quality of welded joints. Experiments were performed with rolled sheets 2, 4 and 6 mm thick, plates 12, 35 and 45 mm thick and press strips up to 140 mm thick. The strength, yield point and impact toughness were determined for various specimens. It was found that the sheets had the greatest density and uniformity of structure, with a few accumulations of intermetallides, primarily in the central portions of the slabs. The macrostructure of the press strips consisted of several zones: a peripheral zone up to 10 mm thick with fine crystalline structure and dispersed intermetallic inclusions, an intermediate zone with alternating deformation strips and oriented accumulations of intermetallides, and a central zone with a coarser structure and accumulations of intermetallides. The specimens contained finely dispersed segregations of hardening phases plus large, individual inclusions or chains of intermetallides measuring up to 0.1 mm. Analysis of the microstructure showed that the rolled sheets had the greatest dispersion of intermetallides. Heterogeneity in distributions of the small hardening phases was greater in the plates and press strips, in which they formed a banded structure. The intermediate and central parts of the press strips contained oriented accumulations of intermetallides, while the peripheral portions contained smaller, more uniformly distributed accumulations. The press strips had greater anisotropy of properties than the plates. When tested for impact toughness, the sheets failed forming large layers. The fracture surfaces of the plates and press strips showed little delamination. The plates failed primarily by viscous fracture. The press strips when tested in a longitudinal direction showed spalling over almost the entire surface, while in the transverse direction, pit fracture with some spalling was observed. The strength, yield point and impact toughness of the specimens cut from all zones of the press strips were practically identical in the longitudinal directions, less in the transverse direction for the same ultimate strength. After heat treatment of templates 20 mm thick cut from the press strip an increase in strength and yield point was observed to 490.8 and 307.6 MPa in the longitudinal direction, 342.8 and 244.8 MPa in the direction through the thickness of the metal. The impact toughness of specimens in these directions was 7.3 and 1.2 J/cm^2. Electron-beam welding was performed on plates 35 to 45 mm thick in a single pass after removal of 0.5 mm from the ends of the plates. Hardness measurements showed that the softened zone measured 32 to 37 mm, with 10 to 5 percent softening. The hardness was HRB 85 to 87. Specimens cut from the peripheral zone were 20 to 25 percent stronger than from the central zone of the press strips with identical yield point. Half of the specimens failed through the thermally affected zone, the others through the melted zone. The heterogeneity of the structure in the melted zone thus resulted in a loss of strength, with accumulated intermetallides acting as stress concentrators. The structural factor is important in determining the toughness characteristics. Figures 5; References 4: Russian.

Analysis of Change in Transverse Deformation of Metal in Seam Zone Upon Argon-Arc Welding of Aluminum Alloys

917D0030C Kiev AVTOMATICHESKAYA SVARKA in Russian Jun 90 pp 19-22

[Article by N. I. Semenyuk and D. M. Rabkin, Institute of Electric Welding imeni Ye. O. Paton, Ukrainian Academy of Sciences]

UDC [621.791.754'293.053:669.715]:539.38

[Abstract] During crystallization, the metal of a welded seam, with little relative elongation, experiences shrinkage and is exposed to welding deformations. Even a slight tensile stress during this period can result in the formation of solidification cracks. Previous works have concluded that for aluminum alloys transverse compression of the metal beyond the welding bath is typical. As the welding speed increases, the compression peak is shifted toward lower temperatures. Selection of an optimal welding mode to prevent solidification cracking requires a study of the changes in transverse deformation of the seam metal in the solid-liquid state. This article

presents an experimental study of the changes in transverse movement in the same zone during crystallization in argon-arc welding of the widely used AD0 alloy as well as type 1420 and AMg6 alloys. Plates measuring 180*150 mm 2 to 4 mm thick were studied. Holes were punched 70 mm from the location of the seam to be made and tungsten rods 0.8 mm in diameter were driven in. The rods mated with holes in the bed of the welding installation to allow measurement of the transverse movements occurring during welding. The specimens were welded with a type EVI-1 tungsten electrode 4 mm in diameter. The results indicated that butt welding of aluminum plates with no gap resulted in an increase in the base distance as the arc approached the section analyzed due to expansion of the heated metal. The base distance then decreased and increased once more as the bath passed due to the increase in volume caused by the addition of the welding wire. The base distance then decreased. It is the moment when the base points start to move together again which is of the greatest interest from the standpoint of the possibility of forming solidification cracks in the welded seam. If the base distance remains unchanged during crystallization, this indicates that tensile stresses are present, creating the danger of formation of solidification cracks. An oscillograph recorded during welding at 10 m/hr indicates tensile deformation during the period when the metal is in the solid-liquid state. At 20 m/hr the solidifying metal undergoes compressive deformation, increasing the resistance to the formation of these cracks. At 30 m/hr the compressive deformations are less or disapper completely, increasing the resistance to formation of solidification cracks in comparison to 10 m/hr, though not as much as at 20 m/hr. Figures 4; References 11: 5 Russian, 6 Western.

Influence of Low-Frequency Modulation of Rectangular Current on Seam Metal Structure in Aluminum Alloy Welding

917D0030D Kiev AVTOMATICHESKAYA SVARKA in Russian Jun 90 pp 23-26

[Article by A. Ya. Isshchenko, A. G. Poklyatskiy, A. V. Lozovskaya, M. R. Yavorskaya, and Ye. M. Slavova, Institute of Electric Welding imeni Ye. O. Paton, Ukrainian Academy of Sciences, V. A. Andreyev, B. P. Rzhanov, "Yuzhnoye" Production Association, Dnepropetrovsk]

UDC [621.791.754'293.053:621.3.014.33:669.715]:620.18

[Abstract] Convincing results have recently been obtained confirming the advantages of pulsed-arc welding of aluminum alloys with infusible electrodes. Equipment has been developed to create welding current pulses allowing the force of the arc to be varied. This article studies the influence of low-frequency modulation parameters of a rectangular alternating welding current produced by a type I-126 power supply on the melting power of the arc and the structure of the metal seam produced in AMg6 alloy. In order to produce a welding current with low-frequency pulsation a modulator was added to the power supply allowing welding in intermitent pulse mode. The pulses and pauses can be varied in length between 60 and 1000 ms, supporting a welding current modulation frequency of 0.5 - 8.3 Hz. AMg6 specimens measuring 400*80*8 mm were tested with a constant arc movement speed of 10 nm/hr, arc length 3 mm, argon flow 20 l/min, electrode diameter 6 mm. The size of the melted zone and structure of the seam metal were determined using specimens cut from the middle parts of the seams. Analysis of the results obtained shows that increasing the length of a pulse sharply increases the melting depth. The seam width changes little. Maximum melting depth is therefore achieved with minimum pause length. However, changing the ratio of pulse to pause length changes the solification conditions in the welding bath and therefore changes the structure of the same metal. Under ordinary conditions there is a moving equilibrium between the influx of heat and its loss into the metal, which forms a directed structure. In pulsed-arc welding this equilibrium is periodically disrupted. With longer pulses the crystallization process approximates that of continuous welding, producing a cellular-dendritic structure. With increasing pause length, the melt spends more time in the supercooled state. As a new pulse is applied, some of the solidified metal is remelted, forming new active crystallization centers, and layers with crystals which are finer in the melted zone and coarser toward the middle of the seam are formed. With a pulse/pause length ratio of about 2/1 a layered structure is formed without a central crystal. Further increases in pause length facilitate a finer structure by activating crystallization centers due to a decrease in the melt temperature. Crystallization is also influenced by the pulse repetition frequency, an increase to 5 Hz allowing the same structural finest to be achieved with shorter pauses. Similar melted metal structures were observed when the pulse length was 150 ms, with pause lengths of both 900 and 56 ms. With identical length of pulses and pauses the size of the melted zone is virtually independent of modulation frequency. However, with equal lengths individual central crystal fragments are always observed in the seam. Figures 5; References 6: Russian.

Influence of Pulsating Arc Welding Mode Parameters in Argon on 1420 Alloy Joint Porosity

917D0030E Kiev AVTOMATICHESKAYA SVARKA in Russian Jun 90 pp 27-30

[Article by R. V. Ilyushenko, Institute of Electric Welding imeni Ye. O. Paton, Ukrainian Academy of Sciences]

UDC [621.791.754'293:621.3.014.33:669.715].002:620.192.47

[Abstract] An analysis of works studying the weldability of type 1420 aluminum-magnesium-lithium alloy indicates that the basic cause of pore formation is that there

are hydrated lithium oxides and other complex hydrogen-containing compounds in the surface layers of welded semifinished goods, which decompose upon heating to liberate gases. This article presents an experimental determination of the optical relationships of parameters of the asymmetrical rectangular current facilitating effective degasing of the welding bath. A special I-126 power supply was used allowing independent control of current in both directions between 100 and 450 A, as well as the length of pulses of current in both directions in the range of 3 to 15 ms. The welding current was modulated at 0.5 - 8.0 Hz by formation of trains of pulses of various amplitudes. Experiments were performed on sheets of 1420 alloys 6 mm thick. Sheets were welded both after hardening and after subsequent artificial aging. The SvAMg63 welding wire was chemically etched before welding to remove a surface layer of 0.01 mm. The porosity of the welded joints obtained was estimated by X-ray studies, analysis of longitudinal and transverse sections and fractures, as well as hydrostatic weighing of seam sections. The results indicated that asymmetry of the welding bipolar current helped to reduce seam porosity. Denser seams were produced by welding under conditions with predominant reverse polarity, which yielded porosities 3 to 5 times less than that of seams made with balanced welding currents regardless of whether the amplitude or length of the current predominated in reverse polarity. Reverse current facilitates rapid breakdown of the surface oxide film on aluminum alloys by cathode atomization. This creates favorable conditions for direct liberation of hydrogen from the surface layers of the metal in molecular form, bypassing dissolution. The experiments yielded dense, practically pore-free welded joints without extensive surface treatment of blanks. Figure 1; References 8: Russian.

Weldability of Dissimilar Aluminum Alloys

917D0030F Kiev AVTOMATICHESKAYA SVARKA in Russian Jun 90 pp 33-36

[Article by V. V. Grinin, V. V. Ovchinnikov, "Znamya truda" Machine-Building Plant, Moscow, V. I Lukin, Ye. N. Ioda, Scientific-Production Association, All-Union Institute of Aviation Materials]

UDC 621.791.754'293.011:669.715:620.192.3

[Abstract] A study is presented of the weldability of dissimilar, deformed and cast aluminum alloys in various combinations, as well as the strength and corrosion properties of their welded joints. The following combinations of alloys were studied: 1201 + VAL10, 1201 + VAL8, AMg6 + VAL8, AMg6 + AL10, AMg6 + VAL14, AMg6 + AL2, AMg3 + AL2, 1420 + VAL8, 1420 + VAL10, 1420 + AMg6. The weldability of alloys in these combinations was studied for manual and automatic argon-arc welding with tungsten electrodes on plates measuring 300×100×2 mm of the cast and deformed metal. The plates were mechanically milled, degreased with acetone or gasoline before welding. The edges to be welded were first scraped. The welding wire used was series-produced wire according to standard GOST 7871 - 75. The surfaces were prepared by etching in NaOH and clarified in HNO_3. Type 1420 alloy was chemically milled to a depth of 0.2 mm on both sides. The hot-crack formation tendency, mechanical properties, corrosion resistance and resistance to corrosion cracking were determined. Overall corrosion resistance was measured by emersion in 3 percent ml containing 0.1 percent H_2O_2. The hot-crack testing showed that when deformed alloys were welded with VAL10 casting alloy this tendency was quite high. Best results were obtained by the use of SvAK5 welding wire for AMg3 + AL2 and AMg6 + AL2. Good seam formation was observed in all cases. The short-term strength was 80 percent of the tensile strength of the weaker of the two alloys welded. Welded joints AMg3 + AL2 (tensile strength 146 MPa) and Amg6 + AL2 (tensile strength 151 MPa) at stresses up to 75 percent of the tensile strength of the welded joint showed no corrosion cracking tendency. The joint of AMg6 + VAL14 had little corrosion cracking tendency. The joints 1420 + VAL8, AMg6 + VAL8, 1201 + VAL8, 1420 + AMg6 had no corrosion cracking tendency. Joints 1201 + VAL10 began to fail after 12 days of testing. Welded joints AMg6 + VAL10 failed after 34 days.

Weldability of High-Strength Aluminum-Zinc-Magnesium Alloy by Electron-Beam Welding

917D0030G Kiev AVTOMATICHESKAYA SVARKA in Russian Jun 90 pp 36-38

[Article by A. A. Bondarev, Institute of Electric Welding imeni Ye. O. Paton, Ukrainian Academy of Sciences]

UDC [621.791.72.011:669.715].001

[Abstract] A study is presented of the strength and ductility of welded joints in a high-strength, thermally hardened aluminum-zinc-magnesium alloy by electron-beam welding. The influence of the use of a filler material and of heat treatment after welding is studied. Studies were performed on plates 32 and 22 mm thick with total content of the primary alloying materials (zinc and magnesium) not over 10 percent . The welding materials used were SvAMg6 wire or a layer of AMg6 alloy. The specimens were chemically etched in 15 percent caustic soda at 50°C and clarified in 30 percent nitric acid before welding. The edges and adjacent areas up to 10 mm wide were scraped to remove all traces of mechanical working immediately before placement in the welding chamber. Specimens were welded in the state after hardening and artificial aging on type U-3M2 and U-212M installations using power supplies which created accelerating voltages of 30 and 60 kv. The pressure in the chamber was about 26.6 MPa. The welding gap was not over 0.15 mm. The short-term strength, yield point, relative elongation and reduction in area of the welded joints were determined using circular specimens 6 mm in diameter cut across the

seam. The impact toughness was determined on 10x10 mm specimens with a Menage notch both in the seam metal and in the melted zone. The welding conditions were adjusted to assure complete melting of the plates with the minimum value of running energy and satisfactory formation of welded joints. Mechanical testing showed that the strength ratio of welded joint to base metal after welding was 0.85. After artificial aging by heating to 170°C, holding 2 hours, this increased to 0.92. When no welding filler material was used the relative elongation of the welded joint was significantly less than that of the base metal, while the other characteristics such as reduction in area and impact toughness changed little. The use of SdAMg6 welding wire or the Mg6 layer reduced the relative strength to 0.7, with the short-term strength and yield point being virtually the same. However, the use of the wire had a positive influence on impact toughness. Hardness testing indicated the formation of zones of incomplete hardening and annealing near the same, with higher hardness. The maximum width of the softened zone was 13 to 14 mm with running energy 10875 J/cm, 6 to 8 mm with running energy 4854 J/cm. Artificial aging restored the hardness of the metal in the zone of thermal influence to that of the base metal, while the seam zone continued to be HRB10 lower than the base metal. As welding speed was increased, the evaporation of elements with high vapor tension decreased. The concentration of magnesium corresponded to its content in the base metal at 26 to 60 m/hr, while the quantity of zince decreased by 10 to 20 percent . The content of the remaining alloy elements remained unchanged. Figures 3.

Influence of Interstitial Impurities on Toughness of Seam Metal in Kh15N6M

917D0028F Kiev AVTOMATICHESKAYA SVARKA in Russian Jun 90 pp 27-30

[Article by A. S. Zubchenko, Scientific-Production Association, Central Scientific Research Institute of Heavy Machine Building, Z. Ya. Gronzal, "Izhorskiy zavod" Production Association, Zh. A. Lepilina, All-Union Scientific Research and Development Institute for Heavy Petrochemical Equipment, I. I. Zhukova, Volgograd State Pedagagic Institute]

UDC [621.791.75.053:669.15'26-194]:669.785:620.17

[Abstract] The variable composition method is used with electron-beam vacuum welding, arc welding by an infusible electrode in argon with various gas flow rates, automatic arc welding under various fluxes is used to study the influence of carbon, nitrogen and oxygen on the structure and properties of Kh15N6M seam metal. Welding with an infusible electrode in argon and automatic arc welding under flux were performed using wire 2 and 4 mm in diameter made of metal produced in a laboratory vacuum-induction furnace. The base metal consisted of plates measuring 500x100x20 mm of O1Kh14N5-VI steel. The impact toughness of the seam metal was determined, hardness was measured and the content of alloy elements in the base metal and seam metal, content of carbon and sulfur, the concentration of nitrogen and oxygen gas were all determined. Fracture surfaces were examined by an electron microscope using single-state carbon replicas. The phase composition was determined by a magnetometric method, the content of residual austenite fine structure parameters by X-ray structural analysis. The deviations in the content of the basic alloy elements did not exceed + 0.3 percent Cr, + 0.092 percent Ni and + 0.02 percent Mo. A plate and wedge were melted by electron-beam welding to vary the composition of the seam metal. The welding condition assured complete melting of the plate and wedge in a single pass. It was found that with a carbon content of over 0.02 percent the impact toughness of the seam metal dropped both in the initial state after welding and after various types of heat treatment. Nitrogen, increasing from 0.005 to 0.040 percent , also decreased the toughness of the metal, though to a significantly smaller extent than carbon. The joint influence of carbon and oxygen on seam metal toughness was evaluated by arc welding at 20, 10 and 5 l/min argon flow rate and electron beam welding in a vacuum. X-ray structural analysis showed that the parameters of the welding process determining the nitrogen and oxygen content in the seam metal qualitatively and quantitatively influence its phase composition and fine structure. Immediately after welding with argon flow rate 10 and 5 l/min an austenite component was found in the seam. The maximum residual austenite is formed with the minimum content of impurities. Increasing the concentration of nitrogen and oxygen decreases A_{c1}. Higher values of impact toughness are achieved by welding with an infusible electrode under argon and by electron-beam welding, a direct result of the lower content of the oxygen and nitrogen interstitial impurities. The total content of carbon and nitrogen in the welding wire should not exceed 0.025 percent, and the welding method used must assure the minimum concentration of oxygen and nitrogen in the seam metal. Automatic arc welding under flux and infusible electrode welding under argons when these conditions are met can achieve impact toughnesses of the seam metal at 293 K of at least 0.5 MJ/m^2 immediately after welding, at least 0.9 MJ/m^2 after high tempering. Figures 5; References 6: Russian.

Abstracts From ELEKTRONNAYA OBRABOTKA MATERIALOV

917D0079A Kishinev ELEKTRONNAYA OBRABOTKA MATERIALOV in Russian No 4, 1990 pp 86-89

[Abstracts of articles appearing in ELEKTRONNAYA OBRABOTKA MATERIALOV, No 4, 1990]

[Text]

UDC 621.9.047;621.352

Amplitude-Time Characteristics of Anode Polarization Rise and Fall Under Conditions of Pulsed Electrochemical Machining. A. V. Rybalko and S. I. Galanin, pp 3-7

This paper discusses the dynamics of the rise and fall of the polarization of metallic anodes by square pulses of current of various amplitudes. It is shown that it is possible to create a nonequipotential anode surface by the purposeful selection of pulse parameters and of the pause between pulses. Experimentally obtained relationships are presented between the peak current density and time for reaching the polarization maximum and the polarization relaxation time—the measure of polarization—for anodes made of the materials 12Kh18N9T, KhN77TYuR and ZhS6KP in aqueous solutions of NaCl and $NaNO_3$ and mixtures of various concentrations with no restrictions on the course of the electrochemical process. The data presented can serve as a basis for setting the conditions for precision electrochemical machining. Figures 9, references 7.

UDC 621.9.047.7

Calculation of Surface Microroughness Parameters in Electrochemical Machining of Structural Steels. Yu. A. Belobragin, V. P. Repin, and N. Ye. Guchek, pp 7-12

It is shown that it is possible to determine a surface's microroughness parameters in electrochemical machining by mathematical modeling of the process of formation of the surface's relief. Polarization, metallographic and X-ray structure studies of machined materials were conducted in order to determine the parameters entering into the model. The results of theoretical calculations showed satisfactory agreement with the experimental data. Figures 4, references 9.

UDC 621.922.34

Acoustic Diagnosis of Process of Electron Discharge Dressing of Diamond Cutting Wheels in Groove Machining. B. V. Morozov, A. M. Senichev, and V. V. Kostin, pp 12-14

A technique is suggested for acoustic diagnosis of the process of the electron-discharge dressing of diamond cutting wheels in the machining of grooves in parts made of nonerrous materials. A determination is made of the life of a wheel that maintains its cutting capabilities without dressing. Figures 3, references 6.

UDC 621.785.54

Laser Surface Hardening of Nickel-Base Alloy With High-Melting Carbides. T. V. Gulyayeva, V. V. Shibayev, S. V. Novikov, and A. N. Safonov, pp 15- 18

A study is made of the structure, geometrical dimensions and properties of areas of the laser surface hardening of a nickel-base alloy. A relationship is established between the properties of the irradiated areas, and laser surface hardening conditions and the types of impregnating compounds and binder components in the surface hardening compound. It is shown that laser surface hardening (reinforcement) with carbide particles, regardless of the type of binder, is realized only during irradiation under conditions when the surface melts. However, the microhardness values of the hardened areas are significantly lower than the hardness of the original carbide materials. It is established that hardening under laser surface hardening can occur both on account of impregnation of the solid solution with carbide decomposition products—Me and C—and on account of the introduction of the original carbide particles into the molten metal. Figures 4, tables 3, references 6.

UDC 620.197.1:621.794:669.295...691.5

Formation of Rutile and Anatase During Microarc Oxidation of Titanium in Water Electrolytes. P. S. Gordiyenko, O. A. Khrisanfova, T. P. Yarovaya, A. G. Zavidnaya, and T. A. Kaydalova, pp 19-22

Coatings consisting of rutile and anatase titanium dioxide and a mixture of these modifications formed on type VT1 - 0 titanium under sparking conditions. It is shown that the electrolyte's anion composition and the pH of the area near the anode exert an influence on the formation of one phase or another of titanium dioxide. Treatment of the surface of titanium by the MDO [micorarc oxidation] technique in electrolytes of a certain anion composition makes it possible to produce protective coatings having prescribed properties. Figures 1, tables 1, references 14.

UDC 669.14.018.8:539.4.015

Combining Ordinary (Cold) and Electroductile Drawing of Steel Wire. O. A. Troitskiy, V. G. Ryzhkov, N. Ye. Kiryanchev, Yu. V. Baranov, and Yu. V. Nikitenko, pp 23-25

It has been learned that by combining ordinary and electroductile drawing (EPV) it is possible to produce a strong and ductile wire from metastable austenitic steel, as well as more stable mechanical properties for the wire as compared with ordinary drawing. Type 18Kh15N5AMZ steel wire 0.95 mm in diameter was drawn by four processes: a) cold drawing (KhV) without current to the breaking instant; b) EPV to a dimension of 0.15 mm; c) EPV to a dimension of 0.47 mm followed by KhV to a dimension of 0.15 mm; and EPV to a dimension of 0.36 mm followed by KhV to a dimension of 0.15 mm. Wire that had undergone cold drawing was most strongly hardened. Its ductility was completely exhausted with a total reduction of 85 percent. In the dimension of 0.24 mm reached, σ_v [ultimate strength] = 2840 MPa and the ductility index was C = 25 percent with a variation factor of 3.6 percent (σ_v). The high stability of the strength indicators of a wire that underwent drawing with the effect of current (or combined drawing) indicates that EPV is conducive to the finely divided, uniform and later, with respect to degrees of reduction, formation of reduction martensite (the alpha phase). Thus, in the course of combining EPV and KhV it is possible to produce a stainless steel wire having especially great strength and fairly great ductility, i.e., high breaking strength. X-ray studies on a DRON-2,0 diffractometer with the determination of regions of

coherent scattering, microdistortions and physical broadening of (111) and (220) lines showed a substantial change in these parameters with EPV as compared with KhV, the polarity of the current's effect, and the physicomechanical and structural properties of the wire, interrelated and caused by the presence of current in the reduction area and its direction relative to the moving reduction area. Figures 4, references 10.

UDC 541.8.661.185:537

Elektrokinetic Phenomena at Phase Interface of Solution of Ionogenic Surface-Active Agent and Air. V. Discussion of Results of Comprehensive Experiments and Theoretical Studies. T. Z. Sotskova, V. Ya. Poberezhnyy, and L. A. Kulskiy, pp 26-30

This paper discusses the results of comprehensive research, based on electrokinetic and adsorption measurements, on the electrical surface properties of the phase interface between an ionogenic surface-active agent and air. Values of the equilibrium ψ_1-potential calculated according to adsorption data with the enlistment of the DES [not further identified] model, consistent with the modified Gouy- Chapman theory, are compared with values of electrokinetic potentials obtained on the basis of measurements of the electroosmosis rate, Dorn potential and electrophoretic mobility of a gas bubble. It is concluded that the DES model used is sufficiently correct and can be used to interpret electrical surface phenomena at the phase interface between an ionogenic surface-active agent (IPAV) solution and a gas. Features of DES polarization at a moving liquid-gas phase interface at the time of electrokinetic measurements are discussed. Figures 1, tables 1, references 21.

UDC 532.5:536.7:537.5

Drop Behavior of Electrostatic Monodispersion of Liquids. A. I. Grigoryev, A. A. Zemskov, and S. O. Shiryayeva, pp 31-35

The critical equilibrium form of constriction that binds to the end of a capillary a drop separating in electrical and gravitational fields is calculated from the principle of minimum free energy. It is shown that the critical radius of constriction with which separation of the drop takes place is determined by the liquid's capillary constant, the radius of the capillary and the magnitude of the potential difference applied. The calculated dependences for the size and charge of the separating drop agree with the experimental data. Figure 6, references 7.

UDC 621.319.7.001.24

Role of Electrode Material in Process of Charging and Separation of Particles from Electrode in Electric Field of Separator. A. R. Gorgoshidze and V. S. Morozov, pp 35-37

This paper presents the data of an experimental study of the adhesion characteristics of the electrodes of electrical separators that separate bulk materials according to conductivity. The probability of the separation of particles is used as the adhesion characteristic. Measurements were made with particles of titanium-containing minerals and spherical metallic particles of nickel. The necessity of making conductivity separator charging electrodes out of graphite-containing materials is proven. Figures 1, tables 2, references 6.

UDC 621.353

Influence of Surface-Active Agent on Substructure of Electrodeposited Copper. O. I. Lyubchik, V. M. Kozlov, and V. K. Sidelnikov, pp 37-40

As study is made by X-ray structure analysis of the influence of certain polyacrylamide and polyethylene glycol surface-active agents on dislocation density and growth twin concentration in electrolytic deposits of copper. In order to explain the relationships obtained, an analysis is made of features of electrolytic nucleation in the presence of molecules of surface-active agents adsorbed on the octahedral plane of a face-centered cubic crystal. It is shown that it is possible for two types of nuclei to originate, differing in the nature of their union with this face. A discussion is presented of the mechanism of the formation of substructural dislocation and twin defects in coatings at the electrolytic nucleation stage during electrodeposition from electrolytes containing surface-active agents. Figures 2, tables 2, references 14.

UDC 620.187.2:542.67:538.2

Use of Models of Exponential Absorption in Magnetic Filtration Removal of Needle-Shaped Particles From Liquids. A. V. Sandulyak, O. Yu. Korkhov, and Yu. G. Kovbasyuk, pp 40-42

This paper presents experiments in the magnetic filtration removal of needle-shaped particles from a water suspension. It is shown that it is possible to use the models, defined earlier, of an exponential (polyexponential) absorbing screen and their main corollaries for the selection of removal conditions and for estimates of the magnetic deposition properties of the particles' dispersed phase. Figure 4, references 1.

UDC 537.226.83

Effect of Electric Field on Jet of Liquid. V. K. Koyekin, pp 43-45

This paper examines the problem of the stability of a jet in an electric field (EP) directed along the axis of the jet, which is discharging upward. It is established experimentally that the jet oscillates in a weak electric field (strength of E approximately equals 200 V/cm). The jet is atomized into small drops when the electric field is intensified to E approximately equals 1.5 kV/cm. Calculations are made of a drop's period of oscillation and of the electric field strength with which a jet of liquid atomizes. Figures 2, references 4.

UDC 621.9.047.7

Influence on Reduction Rate of Chromium (VI) of Products of Electrochemical Treatment of Heat-Resistant Chromium-Nickel Alloys in Nitrate Electrolytes. L. V. Saltanovskaya and A. I. Dikusar, pp 46-49

This paper discusses features of the influence on the kinetics of the reduction of chromium (VI) by means of hydrazine hydrate, of products (both dissolved and present in the solid phase (sediment)) of the high- speed anodic dissolution of chromium-nickel alloy EI-893. It is shown that soluble products of chromium-nickel alloy EI-893 practically do not influence the kinetics of the reduction of chromium (VI) with a pH equal to 2, 7 and 8. The somewhat higher than usual rate of reduction of chromium (VI) in the pH = 5 range in technical-grade solutions is explained by the presence in the solution of molybdenum (VI), which is a catalyst for this reaction. It is learned by a study of the kinetics of the desorption of chromium (VI) and molybdenum (VI) from the sediment studied that a certain amount of both chromium and molybdenum is found in the sediment in the physically adsorbed state, i.e., 13 percent chromium (VI) and 11 percent molybdenum (VI). When reagent techniques are used for the separation of chromium (VI) from the electrolyte, this should result in their desorption into the electrolyte to concentrations corresponding to the equilibrium state. It is shown that the reduction of chromium (VI) in a technical-grade solution containing a sediment must be done with an extra quantity of the reducing agent in order to allow for the portion of chromium (VI) present in the physically adsorbed state in the sediment. Figures 5, tables 3, references 12.

UDC 536.212.621.791.793

Calculation of Temperature Fields in Pulsed Arc Welding. L. D. Kazmina, T. G. Shigayev, and S. K. Khamitov, pp 50-52

This paper presents an analytical study of the temperature field in a weld formed by a pulsed arc. The results obtained make it possible to determine the temperature field in a weld as a function of welding process parameters (rate of travel of the source, its heat ouput and the process's rigidity) and the thermophysical characteristics of the metal being welded. Knowledge of these fields makes it possible to set welding conditions that guarantee the required thermal cycle. The mechanical properties of a welded joint of metals that have undergone structural transformations under intense heating and subsequent cooling depend on the parameters of this thermal cycle. Figures 1, references 3.

UDC 577.3.04

Radiotaxis of Cells of Alga *Dunaliella viridis*. Yu. N. Levchuk, A. I. Karachentseva, and Ye. A. Andreyev, pp 53-57

The phenomenon of negative radiotaxis (mainly motion along the electromagnetic field gradient) was detected in cells of *Dunaliella viridis* under the effect of an electromagnetic field having a frequency of 37.5 GHz. The effect was detected in a laser correlation quasi-elastic-scattered-light spectrometer. Computation of spectral distribution parameters by the method of cumulants showed a reduction in spectral intensities and a change in the effective size of scatterers in all cases of the effect of the field except the case when the cell culture was in the logarithmic phase of growth. It was proved by means of special experiments that the phenomenon observed is not associated with thermal effects. Figures 4, tables 4, references 12.

UDC 628.518.537.2

Systems for Automatic Neutralization of Static Electricity Charges. B. K. Sushko and R. Z. Bakhtizin, pp 58-61

This article describes a closed system for controlling a high-voltage neutralizer of static electricity charges that reacts to changes in the level and sign of the charge being neutralized. The system contains a device for measuring the electrostatic field's strength, whose output is connected to a unit for controlling the operation of the high-voltage neutralizer's power supply. Circuits are presented for three versions of the design of control units. The control system presented can be used in conjunction with high-voltage, high- or industrial-frequency alternating-voltage neutralizers, as well as with direct-voltage neutralizers, sliding-discharge neutralizers and with electropneumatic static electricity charge neutralizers. Figures 3, references 9.

UDC 621.09.048

One Method of Implementing the Process of Simultaneous Two-Cycle Electron Discharge Machining. M. K. Mitskevich, I. A. Bakuto, and S. N. Terekhov, pp 62-64

One way of implementing the proposed simultaneous multicycle technique of electron discharge machining is examined. It is shown that the total time expenditure will be less than with traditional sequential machining in the case when the pulsed current supplied to the electrode for preliminary machining and for supplying the finishing electrode is shunted via a current-limiting resistor. Figures 1, references 3.

UDC 621.9.048.06:658.274

Electron Discharge Hardening of Hot-Rolling Mill Rolls. A. S. Rudyuk, V. F. Korobeynik, G. S. Abramov, and A. G. Ganzhala, pp 64-68

This paper describes the operating principle of a unit for electron discharge hardening (EIU) of cast iron heavy-section-mill rolls. High- chromium and high-carbon steels and alloys are used as the working electrode (OE) material. Studies were made of mass transfer phenomena. A regression relationship was obtained between the cathode's weight gain and the carbon and chromium concentration in the electrode, the discharge energy and

the number of passes of the working electrode. Laboratory "hot wear" tests of specimens after EIU are shown. The wear resistance of rolls increased by a factor of 1.5 to 2 after EIU with high-chromium electrodes. Figures 5, tables 2, references 5.

UDC 622.777

Electrostatic Sizing of Crushed Materials. A. D. Chaplinskiy, A. I. Angelov, and V. S. Morozov, pp 68-72

This paper gives a concise description of the screen sizing of crushed materials, and notes its shortcomings. The main principles of a new technique for sizing in the electrostatic field of wire-gauze electrodes are presented. The results are presented of experimental studies of the character and mechanisms of the motion of particles in electrostatic sizers having wire-gauze electrodes. The interaction with the sizer's electrodes of a particle moving in the space between electrodes is examined. The influence of the characteristics of the electrodes' sizing surfaces on electrostatic sizing indicators is studied. The advantages of the new technique are noted and promising areas of application of the technique and equipment developed are specified. Figures 5, tables 2, references 3.

UDC 621.375:535.211

Study of Antifriction Properties of Coatings on Aluminum Alloys After Laser Surface Hardening. Ya. D. Kogan, Z. S. Sazonova, and V. D. Aleksandrov, pp 73-74

This paper studies the possibility of improving the antifriction properties of aluminum alloys by laser surface hardening employing various compounds. A wide range of pure materials and compounds has been found that help the formation in a laser radiation field, on the surface of aluminum alloys, of hardened areas characterized by high microhardness. Hardened areas having both a homogeneous and sharply pronounced inhomogeneous structure have been produced by varying the energy parameters of laser units and the fineness of hardening powders of various materials. It has been ascertained that it is feasible from the energy viewpoint to control the degree to which the melt bath is filled with hardening materials. The antifriction properties of hardened surfaces are studied and the dependence of these properties on the degree to which the surface is filled with hardening spots and on the structure's homogeneity in the working areas is examined. Figures 3, references 4.

UDC 537.525.5

Improvement of Efficiency of Extraction of Charged Particles From a Plasma Source Based on Reflector Discharge From Tubular Cathode. V. A. Burdovitsin and M. F. Repin, pp 75-76

This paper ascertains the fact that replacement of the cathode material that results in lowering the discharge's voltage increases the concentration of plasma in the vicinity of the emission opening and the efficiency of the extraction of charged particles from the source. Figures 1, tables 1, references 1.

UDC 684.4.052;621.9.048.7

Choice of Optimal Focal Length in Laser Cutting of Materials Having Various Thicknesses. A. N. Safonov, V. I. Skoromnik, A. V. Kuzmin, and L. A. Kvartsova, pp 76-79

This paper discusses questions relating to the selection of focal lengths that guarantee maximum efficiency in the process of the laser cutting of materials. It has been ascertained based on mathematical modeling of laser cutting that there is a unique optimal focal length for each thickness of the material. A type-size series of focal lengths is suggested for groups of thicknesses of materials, based on minimum efficiency loss and economic indicators, as the result of a numerical experiment conducted according to the mathematical model developed. Figures 4, references 3.

UDC 620.193

Microrelief of Surface When Niobium Is Treated by Chemical and Electrochemical Methods. V. D. Kalugin, Ye. B. Pereverzeva, T. A. Naumenko, and S. A. Shapovalov, pp 79-81

This paper studies the surface's microrelief after niobium has been treated in various chemical and electrochemical etching solutions. A version of the combined treatment of niobium is suggested that incorporates the chemical and electrochemical methods followed by stabilization of the metal's surface from oxidation prior to the electroplating stage. Figures 1, tables 1, references 6.

UDC 621.7/9.044.1

Recycling by Electropulse Method of Below-Standard Ferroconcrete Products. N. T. Zinovyev, B. S. Levchenko, B. V. Semkin, and Zh. G. Tanbayev, pp 81-83

This paper describes equipment for the electropulse recycling of below- standard products. Based on the results of practical work (on prototype equipment), it is suggested that the electropulse recycling of below- standard ferroconcrete products be performed in two steps, comprising recovery of the reinforcing skeleton and complete crushing of the demolition products. It is shown that it is feasible to recycle the reinforcing skeleton and aggregate from the crushed concrete in new ferroconcrete products.

UDC 621.3.023:641.77

Calculation of Power of Microwave Oscillator for Heating Food Products. Yu. V. Klokov and A. M. Ostapenkov, pp 83-84

This paper demonstrates that under certain conditions and assumptions the microwave oscillator can be calculated on the basis of the food product's electrophysical properties. References 5.

Improving the Quality of Manufacturing and Repair of Welded Joints and Structures

917D0045A Kiev TEKHNICHESKAYA DIAGNOSTIKA I NERAZRUSHAYUSHCHIY KONTROL in Russian No 3, Jul-Sep 90 pp 40-44

[Article by A.A. Gruzd and I.V. Parkhomenko (now deceased), UkSSR Academy of Sciences Electric Welding Institute imeni Ye.O. Paton, Kiev]

UDC 621.791

[Abstract] The authors briefly describe current advantages and methods and effects of vibrational (low-frequency acoustic) and ultrasonic (high-frequency acoustic) treatment of welded joints to reduce residual stresses and strains. One such setup is tested; an ultrasound generator connected by waveguide to a deforming element (same profile as the bead) with a 50 to 100 micron air gap over a weld. The device moves over the weld at 15 to 10 m/h and affects an area 15 to 50 mm on either side of it. Ultrasound significantly reduces the residual stresses and, in addition, increased the weld hardness from HRC75 to HRC90 and improved fatigue resistance in St3, AMg6, OT4 and VAD-1 materials. Work is being stepped up on the smaller UZDN ultrasound generators, and even smaller ultrasound generators for automatic and handheld devices are being designed. In particular, multiple impact heads are being studied that will smoothly adjust their positions relative to the weld or part contour to transmit ultrasound. References 6 Russian; figures 4; tables 2.

Investigation of Acoustic Conductivity of Oligomer Epoxide-Based Contact Compounds

917D0045B Kiev TEKHNICHESKAYA DIAGNOSTIKA I NERAZRUSHAYUSHCHIY KONTROL in Russian No 3, Jul-Sep 90 pp 44-48

[Article by T.M Shvets, Z.M. Melnichenko, B.S. Kolupayev, G.I. Chalyuk. and O.M. Voloshin, UkSSR Academy of Sciences Colloidal Chemistry, and Water Chemistry Institute imeni A.V. Dumanskiy, Kiev]

UDC 534.8.081.7

[Abstract] Oligomer epoxides contact compounds are the primary kind in use in acoustic diagnostics today. This article studies one such compound: epoxydiene ED-20, carboxyl-containing butadiene-nitryl rubber SKN - 26 - 1a and electrolytic iron with particle size from 0.3 to 1 micron as filler. The density, sound speed, acoustic conductivity, coefficient of absorption, elastic modulus and bond strength as a function of composition is determined. References 6 Russian; figures 4; tables 1.

An Estimate of the Technological Strengths of Various Methods for Multipass Arc Welding of Thick Pieces of Metal

917D0045C Kiev TEKHNICHESKAYA DIAGNOSTIKA I NERAZRUSHAYUSHCHIY KONTROL in Russian No 3, Jul-Sep 90 pp 48-54

[Article by V.I. Panov, Uralmash PO, Sverdlovsk]

UDC 621.791.052.08:620.179.16

[Abstract] The author reports on improvements to the research of V.V. Bazhenov and A.M. Sokolov utilizing a new weld tester developed by TsNIITmash [Technology and Machine Building SRI (Central)] with a central groove for the weld which can be deformed to concentrate stresses on the bead. The cracks which form are analyzed with the IRT-10 crack development indicator (built by Metallurgy and Materials SRI (Central), Sverdlovsk) for acoustic activity, angle of deformation, crack depth, and width of crack opening. A comparative estimate is made of the best welding methods in terms of these quantities. No one method is best for all, but it does show that welding with adaptor clips minimizes the dimensions of the main cracks. References 2 Russian; figures 6; tables 2.

Realizing the Indicator Approach in Acoustic Emission Monitoring of Welds

917D0045D Kiev TEKHNICHESKAYA DIAGNOSTIKA I NERAZRUSHAYUSHCHIY KONTROL in Russian No 3, Jul-Sep 90 pp 80-87

[Article by A.A. Bogdanov, V.V. Volkov, I.Yu. Iyevlev, Yu.B. Kuznetsov, V.V. Laptev, V.I. Panov and V.A. Starodubtsev, Metallurgy and Materials SRI (Central), Sverdlovsk]

UDC 621.791.052.08:620.179.16

[Abstract] The authors have conducted a series of experiments to determine the optimum choice of technical characteristics and parameters for an indicator-type acoustic emission weld checker that would be portable and easy to use. The authors then introduce a device that realizes the results of this testing: the IRT-10 crack development indicator, incorporating in one housing an annular magnet (as waveguide and fastener to surface), battery, electronics and two indicator dials, coarse and fine, with self-regulation of the sensitivity setting. It is 110 x 90 x 40 mm and weighs 0.6 kg, operates for 200 h on one Krona VTs battery, and can detect and record up to eight cracks per indicator in the frequency range from 50 to 300 kHz, with discrimination threshold of 10^{-2} and 10^{-1} V at 20 dB (maximum) gain. A typical example of its use is presented; the IRT - 10 was spot-welded down 0.4 m from where a repair weld was to be made, and it registered two pulses in channel I during the welding, 1 pulse in channel II 40 min later. Although no cracks could be seen at that time upon visual inspection, two days later a crack 50 mm long was found. References 9: 7 Russian, 2 Western; figures 5; tables 1.

NTIS
ATTN: PROCESS 103
5285 PORT ROYAL RD
SPRINGFIELD, VA 22161

This is a U.S. Government publication. Its contents in no way represent the policies, views, or attitudes of the U.S. Government. Users of this publication may cite FBIS or JPRS provided they do so in a manner clearly identifying them as the secondary source.

Foreign Broadcast Information Service (FBIS) and Joint Publications Research Service (JPRS) publications contain political, military, economic, environmental, and sociological news, commentary, and other information, as well as scientific and technical data and reports. All information has been obtained from foreign radio and television broadcasts, news agency transmissions, newspapers, books, and periodicals. Items generally are processed from the first or best available sources. It should not be inferred that they have been disseminated only in the medium, in the language, or to the area indicated. Items from foreign language sources are translated; those from English-language sources are transcribed. Except for excluding certain diacritics, FBIS renders personal and place-names in accordance with the romanization systems approved for U.S. Government publications by the U.S. Board of Geographic Names.

Headlines, editorial reports, and material enclosed in brackets [ ] are supplied by FBIS/JPRS. Processing indicators such as [Text] or [Excerpts] in the first line of each item indicate how the information was processed from the original. Unfamiliar names rendered phonetically are enclosed in parentheses. Words or names preceded by a question mark and enclosed in parentheses were not clear from the original source but have been supplied as appropriate to the context. Other unattributed parenthetical notes within the body of an item originate with the source. Times within items are as given by the source. Passages in boldface or italics are as published.

SUBSCRIPTION/PROCUREMENT INFORMATION

The FBIS DAILY REPORT contains current news and information and is published Monday through Friday in eight volumes: China, East Europe, Soviet Union, East Asia, Near East & South Asia, Sub-Saharan Africa, Latin America, and West Europe. Supplements to the DAILY REPORTs may also be available periodically and will be distributed to regular DAILY REPORT subscribers. JPRS publications, which include approximately 50 regional, worldwide, and topical reports, generally contain less time-sensitive information and are published periodically.

Current DAILY REPORTs and JPRS publications are listed in *Government Reports Announcements* issued semimonthly by the National Technical Information Service (NTIS), 5285 Port Royal Road, Springfield, Virginia 22161 and the *Monthly Catalog of U.S. Government Publications* issued by the Superintendent of Documents, U.S. Government Printing Office, Washington, D.C. 20402.

The public may subscribe to either hardcover or microfiche versions of the DAILY REPORTs and JPRS publications through NTIS at the above address or by calling (703) 487-4630. Subscription rates will be provided by NTIS upon request. Subscriptions are available outside the United States from NTIS or appointed foreign dealers. New subscribers should expect a 30-day delay in receipt of the first issue.

U.S. Government offices may obtain subscriptions to the DAILY REPORTs or JPRS publications (hardcover or microfiche) at no charge through their sponsoring organizations. For additional information or assistance, call FBIS, (202) 338-6735,or write to P.O. Box 2604, Washington, D.C. 20013. Department of Defense consumers are required to submit requests through appropriate command validation channels to DIA, RTS-2C, Washington, D.C. 20301. (Telephone: (202) 373-3771, Autovon: 243-3771.)

Back issues or single copies of the DAILY REPORTs and JPRS publications are not available. Both the DAILY REPORTs and the JPRS publications are on file for public reference at the Library of Congress and at many Federal Depository Libraries. Reference copies may also be seen at many public and university libraries throughout the United States.